

# Empirical Bayes Shrinkage of Functional Effects, with Application to Analysis of Dynamic eQTLs

Ziang Zhang

Department of Human Genetics, University of Chicago, Chicago, IL

Peter Carbonetto

Department of Human Genetics, University of Chicago, Chicago, IL

Matthew Stephens

Departments of Statistics and Human Genetics,  
University of Chicago, Chicago, IL

February 4, 2026

## Abstract

We introduce functional adaptive shrinkage (FASH), an empirical Bayes method for joint analysis of observation units in which each unit estimates an *effect function* at several values of a continuous condition variable. The ideas in this paper are motivated by dynamic expression quantitative trait locus (eQTL) studies, which aim to characterize how genetic effects on gene expression vary with time or another continuous condition. FASH integrates a broad family of Gaussian processes defined through linear differential operators into an empirical Bayes shrinkage framework, enabling adaptive smoothing and borrowing of information across units. This provides improved estimation of effect functions and principled hypothesis testing, allowing straightforward computation of significance measures such as local false discovery and false sign rates. To encourage conservative inferences, we propose a simple prior adjustment method that has theoretical guarantees and can be more broadly used with other empirical Bayes methods. We illustrate the benefits of FASH by reanalyzing dynamic eQTL data on cardiomyocyte differentiation from induced pluripotent stem cells. FASH identified novel dynamic eQTLs, revealed diverse temporal effect patterns, and provided improved power compared with the original analysis. More broadly, FASH offers a flexible statistical framework for joint analysis of functional data, with applications extending beyond genomics. To facilitate use of FASH in dynamic eQTL studies and other settings, we provide an accompanying R package at <https://github.com/stephenslab/fashr>.

*Keywords:* Multiple hypothesis testing; Gaussian process; Bayesian inference; Adaptive shrinkage; Functional data analysis; Expression quantitative trait locus

## 1 Introduction

Perturbing a system, and measuring the changes that result, is a classic scientific way to understand a system (DeRisi et al., 1997; Heller et al., 1997; Hughes et al., 2000). Modern genomics experiments therefore often measure the behaviors of many genomic units under a variety of perturbations or treatments. Some of these experiments involve measuring how behaviors change as a function of some underlying continuous variable. For example, recent expression quantitative trait locus (eQTL) and allele-specific expression (ASE) studies measure how the effects of genetic variants on gene expression change over time, or with respect to a continuous condition such as oxygen level (Cuomo et al., 2020; Elorbany et al., 2022; Francesconi and Lehner, 2014; Gutierrez-Arcelus et al., 2020; Kang et al., 2023; Nathan et al., 2022; Soskic et al., 2022; Strober et al., 2019). These studies, which we refer to as “dynamic eQTL studies”, typically produce noisy measurements of eQTL effects for genomic units (gene-variant pairs) at multiple settings of a continuous condition. The goals of dynamic eQTL studies include estimating the underlying eQTL effect functions (e.g., to characterize how the eQTL effect changes over time) and identifying which eQTL effects deviate from some “null” or “baseline” behavior. This null or baseline could be defined as no change over time, or a linear change over time.

Dynamic eQTL studies involve massive data, generating noisy measurements from thousands or even millions of genomic units. Therefore, statistical inferences can be greatly improved by sharing information across units rather than treating each unit separately as is typically done. Empirical Bayes (EB) (Efron, 2008, 2009) provides a powerful framework for accomplishing this. EB methods learn a common prior distribution from all units, which is usually centered

on the null or baseline, and then it improves the effect estimates for each unit by shrinking them toward this null. An attractive feature of EB is that the amount of shrinkage is adaptive in that it depends on both the prior distribution (for example, experiments with more null units result in prior distributions that shrink more) and on the standard errors of the effect estimates (the noisier the estimate, the stronger the shrinkage) (Stephens, 2017). EB methods and convenient software implementations are widely available and are becoming more frequently used for studies involving one condition (Stephens, 2017; Willwerscheid et al., 2025) or several conditions (Urbut et al., 2019; Liu et al., 2024).

In this work, we develop new empirical Bayes methods and software for estimating *effect functions* that are defined on a continuously-valued space such as time. To model the effect functions, we use Gaussian processes (GP) (MacKay, 2003), probably the simplest and most widely used approach to define a prior distribution for functions. We exploit a family of GPs which we call the “*L*-GP family” that can encode diverse functional shapes and behaviors. Members of this family are defined by a single scalar parameter,  $\sigma$ , that quantifies deviations from a null/baseline model space (e.g., the space of constant functions or the space of linear functions) (Lindgren and Rue, 2008; Yue et al., 2014; Zhang et al., 2024, 2025). We show how the *L*-GP family can be combined with adaptive shrinkage ideas (Stephens, 2017) to *adaptively shrink functions*. We call the new methods “**F**unctional **A**daptive **S**Hrinkage” (FASH).

The combination of these ideas also provides a flexible way to perform hypothesis testing on effect functions; that is, to assess whether an effect function significantly departs from a given baseline model. Hypothesis testing on effect functions through FASH is very different from—and has important benefits over—the *ad hoc* approaches that have been used in dynamic eQTL studies (Cuomo et al., 2020; Elorbany et al., 2022; Francesconi and Lehner, 2014; Gutierrez-Arcelus et al., 2020; Kang et al., 2023; Nathan et al., 2022; Soskic

et al., 2022; Strober et al., 2019). For example, Soskic et al. (2022) performed hypothesis testing by comparing models of gene expression with and without a genotype  $\times$  time interaction term. The problem with this approach is that it fails to account for other potentially interesting time-dependent effects in which the changes over time are nonlinear. (Recognizing this limitation, Soskic et al. (2022) also compared models with and without a quadratic interaction term, genotype  $\times$  time<sup>2</sup>, but this still makes a restrictive assumption about how the eQTL effects vary with respect to time.) By contrast, the hypothesis testing in FASH does not make such assumptions (see Section 2 for an illustration). As a result, our approach is more flexible and powerful. Furthermore, FASH has another benefit over the approaches that have been used in dynamic eQTL studies: previous approaches involve fitting models using the individual-level data, whereas FASH operates on summary statistics, which are sometimes available when the individual-level data are not (e.g., due to HIPAA requirements or other data privacy concerns). Therefore, FASH can also be applied to settings where only summary statistics are available.

Finally, we note that our new methods also address a well known but often unaddressed limitation of empirical Bayes methods. EB methods generally require that the prior distribution accurately captures both the null and alternative hypotheses to achieve calibrated inference. However, accurately specifying the prior under the alternative is often unrealistic in practice, and the resulting inferences may therefore lose calibration or become anticonservative. To help ensure conservative inferences, we develop a Bayes factor (BF)-based adjustment to the prior. While we only implemented this idea for FASH in this paper, we note that it is a general technique that could potentially be used for other EB-based shrinkage methods.

All the methods described in this paper have been implemented in an R package, **fashr** (“functional adaptive shrinkage in R”), which is available at <https://github.com/stephen-slab/fashr>. To our knowledge, the previous dynamic eQTL studies did not disseminate

dedicated software tools for their hypothesis testing pipelines, so **fashr** represents the first integrated software for dynamic eQTL studies. Further, the FASH method and software implementation are quite general, and therefore we foresee the potential to apply FASH to other data sets beyond dynamic eQTL studies. The R package has detailed documentation and an accessible interface, as well as a vignette illustrating recommended usage of **fashr** for a dynamic eQTL data set.

## 1.1 Organization of Paper

The rest of the paper is organized as follows. In Section 2, we present a motivating example illustrating shrinkage toward a baseline model and adaptive shrinkage via borrowing information across observation units. In Section 3, we introduce our FASH approach together with a BF-based adjustment for conservative hypothesis testing. In Section 4, we apply FASH to reanalyze the dynamic eQTL dataset of Strober et al. (2019), spanning 16 days of cardiomyocyte differentiation from induced pluripotent stem cells and comprising over one million gene–variant pairs. This analysis identifies novel dynamic eQTLs, reveals diverse temporal effect patterns, and provides a more accurate characterization of effect functions than the parametric interaction analysis in the original study, which imposes more rigid assumptions. Finally, Section 5 summarizes our contributions, outlines current limitations of our approach, and discusses potential extensions to other areas.

## 2 A Motivating Example

To motivate the key ideas of our approach, we first give an example from the dynamic eQTL application that is presented in more detail below. For this example, we focus on data and results for a single gene-variant pair: gene *FZD6* and SNP rs28392906. The black dots in each of the panels in Figure 1 show the eQTL effect estimates at the different time points

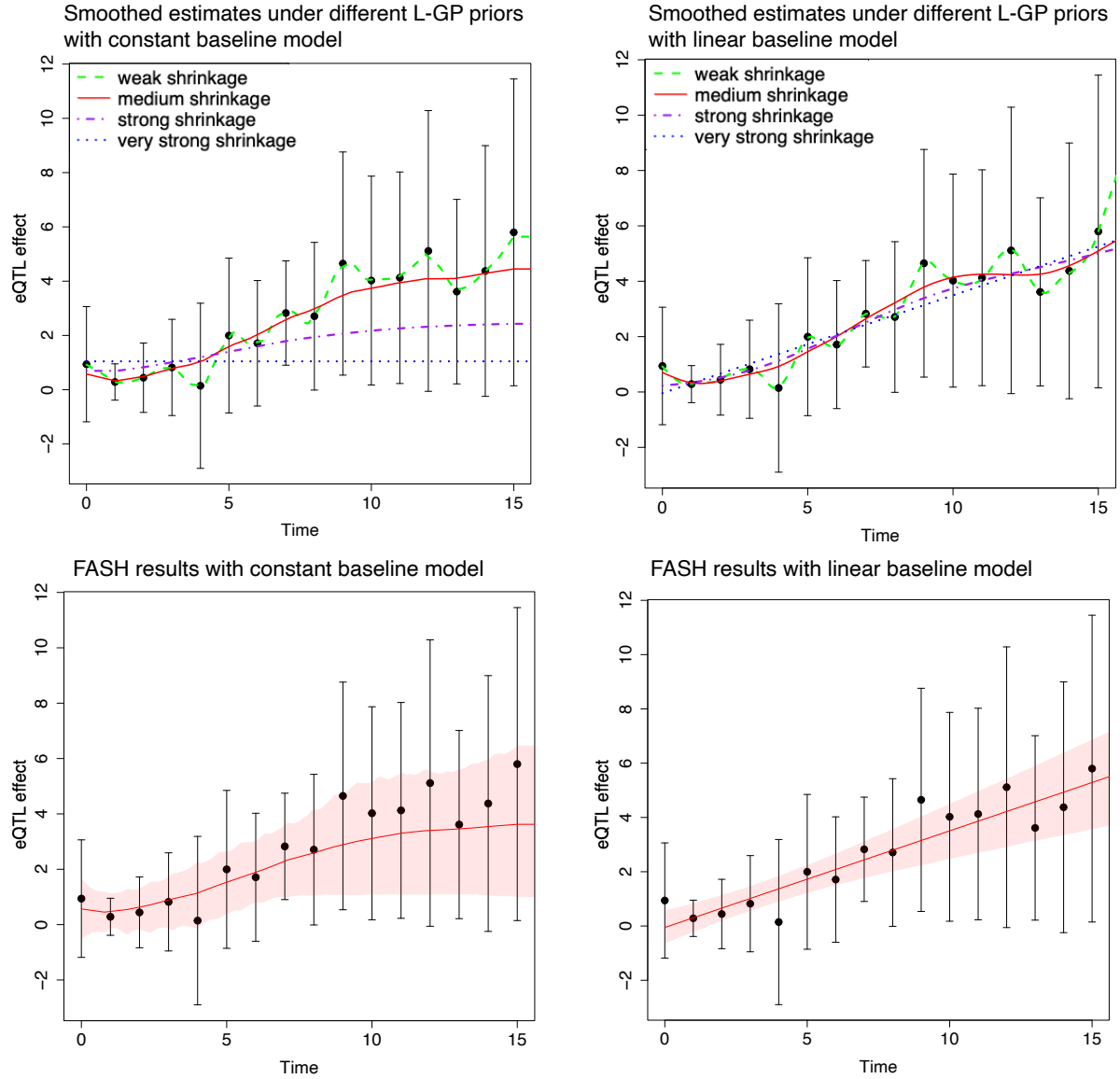


Figure 1: Example illustrating the use of FASH to analyze a dynamic eQTL data set. In all panels, the original eQTL effect estimates are shown as black dots, and vertical error bars depict  $\pm 2$  standard errors. The top two panels show the smoothed estimates defined as the posterior means from the  $L$ -GP method; the different estimates are obtained by different levels of shrinkage toward the constant and linear baseline models (left and right panels, respectively). The bottom two panels summarize the results from the proposed FASH method, with constant and linear baseline models (left and right panels, respectively). The constant and linear baseline models are defined using  $L$ -GP processes with  $L = D^1$  and  $L = D^2$ , respectively (see Section 3.4). The posterior mean effect function is shown as a solid red line; the shaded region shows the 95% credible interval.

for this gene-variant pair. The standard errors of the eQTL effects are shown as vertical error bars.

Part of the statistical analysis involves improving the accuracy of these “noisy” eQTL estimates by shrinking them toward a baseline model. The baseline models in FASH assume that the true effect function under this model varies “smoothly” over time. But the exact baseline model we choose is guided by the scientific question of interest. Here we consider two questions: (i) Is the eQTL effect *dynamic*—that is, does it change over time? (ii) Does the eQTL effect change over time in a way that deviates from a linear trend—that is, does it exhibit nonlinear changes over time? The null hypotheses corresponding to these baseline models are: (i) the effect function is constant; (ii) the effect function is linear. Our methods can shrink the effect functions towards either of these baseline models, as well as other baseline models.

First, to illustrate this smoothing of the effect estimates, we show the result of applying the  $L$ -GP model with different levels of shrinkage, and with either the constant (Figure 1, top-left panel) or linear baseline (top-right panel). From these plots, we see that the smoothed estimates vary greatly depending on the shrinkage level. At the strongest shrinkage level, the smoothed estimates reduce to a constant function that averages across time points or a straight line from weighted linear regression. At the weakest shrinkage level, the smoothed estimates become a curve that interpolates all data points exactly. Thus, determining the appropriate level of shrinkage is critical to the analysis.

The bottom two panels in Figure 1 visualize the posterior distributions of the effect functions obtained by applying FASH to these data. FASH uses  $L$ -GP priors, but adapts these priors to the data by pooling the information from all the available gene-variant pairs. Additionally, the shrinkage level is adapted separately for each gene-variant pair depending on how closely the data match the baseline model; data close to the baseline model tend to be shrunk more strongly than data that are far away. (Different shrinkage patterns for other gene-variant pairs are shown in Section 4). This is sometimes referred to as “global-local” shrinkage

(Polson and Scott, 2010).

In this example, the data are not consistent with a baseline model in which there is no change in the effect over time. Therefore, the estimates are shrunk weakly with respect to this baseline (Figure 1, bottom-left). The hypothesis test from this baseline model is a test of whether the effects remain unchanged over time; clearly, there is strong evidence for rejecting this hypothesis. (Hypothesis testing in FASH is introduced more formally below.) Note that this test does not make any specific assumptions about *how* the effects change over time (unlike analyses in many published dynamic eQTL studies which do make such assumptions).

In the bottom-right panel of Figure 1, we see that the data are much more consistent with a linear change in effect over time. Therefore, the effect estimates are strongly shrunk toward the linear baseline model. Since these data agree well with the linear baseline model, it follows that there is little evidence for rejecting the hypothesis of a linear change in eQTL effects, and therefore we view a roughly linear increase in the eQTL effects over time as a plausible description of these data. The two tests address different questions: the first assesses whether the effects change over time at all, whereas the second assesses whether there is evidence that those changes are nonlinear. We give other examples of hypothesis testing in Section 4.

## 3 Functional Adaptive Shrinkage

### 3.1 Notation

We use the following conventions in the mathematical expressions. For an integer  $J$ , we write  $[J] = \{1, \dots, J\}$  for the index set. For a set  $A$ ,  $|A|$  denotes its cardinality. The normal distribution with mean  $\mu$  and variance  $\sigma^2$  is written as  $N(\mu, \sigma^2)$ , with density

$d\mathcal{N}(\cdot; \mu, \sigma^2)$ . We abbreviate “independent and identically distributed” as “iid”, and we abbreviate “independent” as “ind”. We use  $\mathbb{Z}^+$  to denote the set of positive integers,  $\mathbb{R}$  for the set of real-valued vectors,  $\mathbb{R}^p$  for the set of real-valued vectors of length  $p$ ,  $\mathbb{R}^{p \times q}$  for the set of real-valued matrices of size  $p \times q$ , and  $C^p(\Omega)$  for the set of functions  $\Omega \rightarrow \mathbb{R}$  that are  $p$ -times continuously differentiable.

### 3.2 Problem Setup

Let  $J \in \mathbb{Z}^+$  be the number of observation units. For each unit  $j \in [J]$ , we assume that we have effect estimates at several values of a continuous condition variable  $t \in \mathbb{R}$ . We denote these effect estimates by  $\hat{\beta}_j(t_{j1}), \dots, \hat{\beta}_j(t_{jR_j}) \in \mathbb{R}$ , where  $R_j$  is the number of settings of  $t$  where we have effect estimates for unit  $j$ . *Our main aim is to estimate an underlying effect function  $\beta_j$ , a mapping from  $t \in \Omega$  to  $\mathbb{R}$ .* We are particularly interested in settings where the number of units,  $J$ , is large—say, hundreds or thousands, or perhaps more—so that we can pool information to improve estimation of the underlying effect functions. It is also important that have observations at several values of  $t$  for each  $j \in [J]$ .

In a dynamic eQTL study,  $J$  is the number of gene-variant pairs, and each  $\beta_j(t_{jr})$  is the estimated effect of a genetic variant on gene expression at time point  $t_{jr}$  (or setting  $t_{jr}$  of the continuous variable). When there is only one genetic variant associated with each gene,  $J$  is simply be the number of genes. In our dynamic eQTL case study below (Section 4),  $J$  is over 1 million, and  $R_j = 16$  for all  $j \in [J]$ . Note that in some dynamic eQTL studies, expression is only measured at 2 or 3 time points, which is probably too few for our methods to be useful.

### 3.3 Empirical Bayes for Functional Data Analysis

Our methods assume that the effect estimates are independent and normally distributed given the underlying effect function:

$$\hat{\beta}_j(t_{jr}) \mid \beta_j, s_{jr} \stackrel{\text{ind}}{\sim} N(\beta_j(t_{jr}), s_{jr}^2), \quad r \in [R_j], \quad (1)$$

in which  $s_{jr}$  denotes the standard error of the effect estimate  $\beta_j(t_{jr})$ . We further assume each underlying effect functions  $\beta_j$  are iid draws from a prior distribution for functions on  $\Omega \rightarrow \mathbb{R}$ , denoted by  $g_\beta$ :

$$\beta_j \stackrel{\text{iid}}{\sim} g_\beta. \quad (2)$$

We have two main inference goals:

1. **Smoothing:** Recover and visualize the underlying effect function,  $\beta_j$ , or its functionals (e.g., derivatives), at observed or unobserved values of  $t$ .
2. **Hypothesis testing:** Identify the units  $j$  that deviate from a null hypothesis  $H_0 : \beta_j \in S_0$ , where  $S_0$  denotes some prespecified class of functions. In some applications, we might also be interested in testing hypotheses of the form  $H_0 : \mathcal{F}(\beta_j) = 0$  for some functional  $\mathcal{F} : C^p(\Omega) \rightarrow \mathbb{R}$ . For example, we might be interested in testing whether the maximum of the function exceeds a given threshold  $\alpha$ , which would be achieved with  $\mathcal{F}(\beta_j) = \max_{t \in \Omega} \beta_j(t) - \alpha$ .

The first goal (“smoothing”) will be accomplished by computing the posterior distribution of each effect function  $\beta_j$ :

$$p(\beta_j \mid \hat{\beta}_j, \mathbf{s}_j, g_\beta) \propto p(\hat{\beta}_j \mid \beta_j, \mathbf{s}_j) g_\beta(\beta_j), \quad (3)$$

such that  $\hat{\beta}_j := (\hat{\beta}_j(t_{j1}), \dots, \hat{\beta}_j(t_{jR_j}))^T$ ,  $\mathbf{s}_j := (s_{j1}, \dots, s_{jR_j})^T$  denote the available data for unit  $j \in [J]$ . A smoothed point estimate of  $\beta_j$  can be then obtained by its posterior mean.

The second goal (“hypothesis testing”) is accomplished by computing local false discovery rates and local false sign rates (see below).

Specifying a single prior  $g_\beta$  that works well across all data sets is generally unrealistic, so it is much better if there is a mechanism to learn or adapt a prior automatically based on the data. We take an empirical Bayes approach to learning a prior: given a predefined family of prior distributions,  $\mathcal{G}_\beta$  (which we will define below), we choose a  $g_\beta \in \mathcal{G}_\beta$  that maximizes the log-likelihood of all the data,

$$\hat{g}_\beta = \operatorname{argmax}_{g_\beta \in \mathcal{G}_\beta} \sum_{j=1}^J \log \int \prod_{r=1}^{R_j} p(\hat{\beta}_j(t_{jr}) \mid \beta_j, s_{jr}) \times g_\beta(\beta_j) d\beta_j, \quad (4)$$

and then all subsequent inferences use this estimated prior  $\hat{g}_\beta$ .

Although our main aim is to make inferences about the unknown effect functions, which involves reasoning about probability distributions on functions, the underlying statistical computations are straightforward in practice, reducing to probability distributions on finite-dimensional spaces. Letting  $\beta_j := (\beta_j(t_{j1}), \dots, \beta_j(t_{jR_j}))$  denote the underlying effect function at the values of  $t$  where the effect estimates are available, and  $\beta := \{\beta_1, \dots, \beta_J\}$ , the modeling assumptions above imply the existence of a prior  $p(\beta; g_\beta)$  such that

$$p(\beta; g_\beta) = \prod_{j=1}^J p(\beta_j; g_\beta), \quad (5)$$

where  $p(\beta_j; g_\beta)$  denotes the finite-dimensional distribution on  $\beta_j$  induced by the prior  $g_\beta$ . For example, the statistical computations needed for the maximum-likelihood estimation of the prior (4) reduce to finite-dimensional integrals:

$$\hat{g}_\beta = \operatorname{argmax}_{g_\beta \in \mathcal{G}_\beta} \sum_{j=1}^J \log \int p(\hat{\beta}_j \mid \beta_j, s_j) p(\beta_j; g_\beta) d\beta_j, \quad (6)$$

where

$$p(\hat{\beta}_j \mid \beta_j, s_j) = \prod_{r=1}^{R_j} d\mathcal{N}(\hat{\beta}_j(t_{jr}); \beta_j(t_{jr}), s_{jr}^2). \quad (7)$$

### 3.4 The Functional Adaptive Shrinkage Family of Priors

We now describe the “functional adaptive shrinkage” family of prior distributions on effect functions that addresses the goals outlined above. The construction of this family begins with the specification of a “baseline model,”  $S_0$ . This is done by specifying a  $p$ th-order linear differential operator  $L = \sum_{i=0}^p c_i D^i$ , where  $D^i$  denotes the  $i$ th derivative operator and the  $c_i \in \mathbb{R}$  are specified coefficients. Then we define the baseline model as

$$S_0 = \text{Null}\{L\} = \{\beta \in C^p(\Omega) : L\beta = 0\}. \quad (8)$$

For example, if  $L = D^1$ , then  $S_0 = \text{span}\{1\}$  corresponds to the class of constant functions; if  $L = D^2$ , then  $S_0 = \text{span}\{1, t\}$  corresponds to the class of linear functions. More generally, for  $L = D^p$ , the baseline model corresponds to the space of polynomials of order  $p - 1$ .

Given  $L$ , we define an  $L$ -Gaussian process (“ $L$ -GP”) as a Gaussian process satisfying

$$L\beta = \sigma \xi, \quad (9)$$

where  $\xi$  is standard Gaussian white noise, and  $\sigma > 0$  is a parameter that governs how much  $\beta$  deviates from the baseline model  $S_0$ . For conciseness, we write this as

$$\beta \sim L\text{-GP}(\beta; \sigma).$$

When  $L = D^p$ , the  $L$ -GP corresponds to the  $p$ th-order Integrated Wiener Process (IWP <sub>$p$</sub> ) (Shepp, 1966). The IWP prior is closely connected to smoothing splines as its posterior mean coincides with the spline estimator (Wahba, 1978). In what follows, we focus on  $L$ -GPs of the IWP <sub>$p$</sub>  form, while noting that the method also applies to other types of  $L$ -GPs; see Lindgren and Rue (2008); Yue et al. (2014); Zhang et al. (2024, 2025) for further background and examples.

When using an  $L\text{-GP}(\beta; \sigma)$  prior for  $\beta$ , the choice of  $L$  governs the baseline model toward which shrinkage occurs, and choice of  $\sigma$  governs the level of shrinkage. As  $\sigma$  decreases

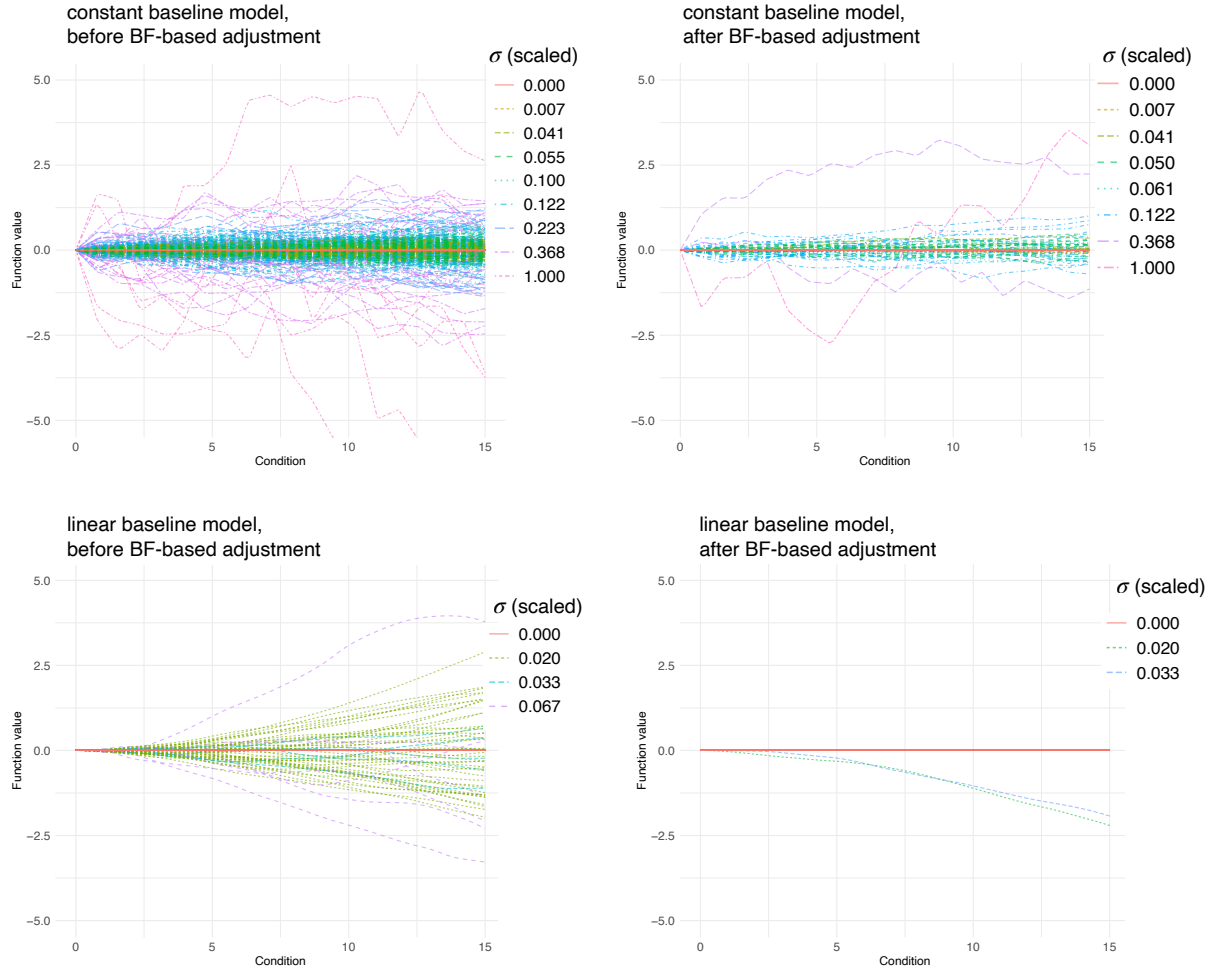


Figure 2: Sample paths randomly drawn from the fitted FASH priors that were estimated from the dynamic eQTL data in Section 4, for  $L = D^1$  (top) and  $L = D^2$  (bottom), before (left) and after (right) the BF-based adjustment. For purposes of visualization, we constrained the sample paths to have an initial condition of zero; that is,  $\beta(0) = 0$  in the top row, and  $\beta(0) = \beta'(0) = 0$  in the bottom row. 5,000 randomly sampled paths are shown in each plot.

toward zero, the  $L$ -GP becomes increasingly constrained to remain close to the baseline model. Figure 2 illustrates how different settings of  $\sigma$  result in different prior distributions on effect functions.

For a flexible family of prior distributions that can appropriately adapt the amount of shrinkage to the data, we use mixtures of  $L$ -GP priors,

$$\mathcal{G}_\beta = \left\{ g_\beta : g_\beta = \sum_{k=0}^K \pi_k L\text{-GP}(\beta; \sigma_k) \right\}, \quad (10)$$

in which the  $\{\sigma_k\}_{k=0}^K$  denote a fixed grid of values ordered from small ( $\sigma_0 = 0$ , corresponding to no deviation from  $S_0$ ) to large ( $\sigma_K$ ), and the  $\pi_k$  denote mixture weights ( $\pi_k \geq 0$ ,  $\sum_{k=0}^K \pi_k = 1$ ). We refer to (10) prior family as the “functional adaptive shrinkage prior” family as its construction mirrors the “adaptive shrinkage priors” from Stephens (2017); Urbut et al. (2019).

Since the priors of the form (10) are fully specified by the mixture weights  $\boldsymbol{\pi} := (\pi_k)_{k=0}^K$ , learning the prior  $g_\beta \in \mathcal{G}_\beta$  reduces to learning the prior weights:

$$\begin{aligned} \hat{\boldsymbol{\pi}} &= \operatorname{argmax}_{\boldsymbol{\pi}} l(\boldsymbol{\pi}), \\ l(\boldsymbol{\pi}) &:= \sum_{j=1}^J \log \left\{ \sum_{k=0}^K \pi_k \ell_{jk} \right\}, \end{aligned} \tag{11}$$

where  $\ell_{jk}$  denotes the marginal likelihood of unit  $j$  under the  $k$ th component of the prior; that is,  $\ell_{jk}$  is the marginal likelihood  $p(\hat{\boldsymbol{\beta}}_j \mid \mathbf{s}_j) = \int p(\hat{\boldsymbol{\beta}}_j \mid \boldsymbol{\beta}_j, \mathbf{s}_j) p_j(\boldsymbol{\beta}_j; g_\beta) d\boldsymbol{\beta}_j$  with a prior of the form (10) in which  $\pi_k = 1$  and the remaining mixture weights are zero.

### 3.5 Posterior Inference in FASH

In addition to computing posterior means, variances and other posterior moments of effect functions, we also use the posterior distributions (12) to perform hypothesis testing on effect functions. All these involve computing expectations with respect to posterior distributions on effect functions (3). Due to conjugacy of the likelihood (1) and the prior (10), the posterior distributions are also mixtures:

$$p(\beta_j \mid \hat{\boldsymbol{\beta}}_j, \mathbf{s}_j, \hat{\boldsymbol{\pi}}) = \sum_{k=0}^K \tilde{\pi}_{jk} p_k(\beta_j \mid \hat{\boldsymbol{\beta}}_j, \mathbf{s}_j), \tag{12}$$

where  $p_k(\beta_j \mid \hat{\boldsymbol{\beta}}_j, \mathbf{s}_j)$  denotes the posterior of unit  $j$  under the  $k$ th  $L$ -GP component, and the  $\tilde{\pi}_{jk}$  denote the posterior mixture weights,

$$\tilde{\pi}_{jk} := \frac{\hat{\pi}_k \ell_{jk}}{\sum_{k'=0}^K \hat{\pi}_{k'} \ell_{jk'}}. \tag{13}$$

Also, the Markovian structure of the  $L$ -GP facilitates efficient computation of these posteriors. We elaborate on this in the Appendix A of supplement.

### 3.5.1 Hypothesis Testing

To test  $H_0 : \beta_j \in S_0$ , a common approach is to control the false discovery rate (FDR) across the  $J$  units, either in the classical frequentist formulation (Benjamini and Hochberg, 1995), or in closely related Bayesian formulations (Storey, 2002; Efron, 2008). For a subset  $\Gamma \subseteq [J]$  flagged as significant, the estimated FDR is obtained from the local false discovery rate (lfdr) (Efron, 2008) as

$$\widehat{\text{FDR}}(\Gamma) = \frac{1}{|\Gamma|} \sum_{j \in \Gamma} \text{lfdr}(j), \quad (14)$$

in which

$$\text{lfdr}(j) := p(\beta_j \in S_0 \mid \hat{\beta}_j, \mathbf{s}_j, \hat{\pi}). \quad (15)$$

Since the  $k = 0$  component of the mixture prior (10) corresponds to  $S_0$ , in FASH the lfdr reduces to

$$\text{lfdr}(j) = \tilde{\pi}_{j0}. \quad (16)$$

For testing hypotheses of the form  $H_0 : \mathcal{F}(\beta_j) = 0$ , where  $\mathcal{F} : C^p(\Omega) \rightarrow \mathbb{R}$  is a functional, there is the potential use local false sign rates (lfsr) and false sign rates (FSR), which are generally more robust than the lfdr and FDR (Stephens, 2017). For a two-sided alternative  $H_1 : \mathcal{F}(\beta_j) \neq 0$ , the lfsr is

$$\text{lfsr}(j) = \min \left\{ p(\mathcal{F}(\beta_j) \geq 0 \mid \hat{\beta}_j, \mathbf{s}_j, \hat{\pi}), p(\mathcal{F}(\beta_j) \leq 0 \mid \hat{\beta}_j, \mathbf{s}_j, \hat{\pi}) \right\}. \quad (17)$$

For a one-sided alternative, e.g.,  $H_1 : \mathcal{F}(\beta_j) > 0$ , we define the lfsr as

$$\text{lfsr}(j) = p(\mathcal{F}(\beta_j) \leq 0 \mid \hat{\beta}_j, \mathbf{s}_j, \hat{\pi}). \quad (18)$$

The cumulative FSR can be computed from the lfsr analogously to the FDR (Stephens, 2017).

### 3.6 BF-based Adjustment of $\hat{\pi}_0$

The lfdr and FDR can be quite sensitive to the estimate of the null proportion,  $\pi_0$ . Although lfsr and FSR are generally more robust than lfdr and FDR, they can still be influenced by the estimate  $\hat{\pi}_0$ . In particular, if  $\hat{\pi}_0$  falls below the true  $\pi_0$ , inference can become anti-conservative, resulting in an inflated FDR or FSR. Consequently, a conservative estimate, in which  $\hat{\pi}_0 \geq \pi_0$ , would be preferred.

One major reason for underestimating  $\hat{\pi}_0$  in FASH is misspecification of the prior family; if the mixture prior family (10) is not sufficiently flexible to approximate the true marginal distribution, then the maximum-likelihood estimate of  $\pi_0$  can become inaccurate. In the simpler univariate setting (Stephens, 2017), prior misspecification may be a mild concern, but in FASH, like in other multivariate settings (Urbut et al., 2019; Liu et al., 2024), the concern is greater due to the difficulty of adequately modeling data in high dimensions.

To guard against this issue, we describe a simple yet effective BF-based adjustment of  $\hat{\pi}_0$ . This adjustment is not specific to FASH, and could potentially be used in other settings where prior could be misspecified. This adjustment only exploits the fact that, under the null hypothesis, the BF in favor of the alternative has an expectation of 1 (that is, BFs are *e*-variables; see Vovk and Wang 2021). This property of BFs is stated more formally in the following lemma.

**Lemma 1:** Let the Bayes factor for unit  $j$  be

$$\text{BF}_j := \frac{p_1(\hat{\beta}_j \mid \mathbf{s}_j)}{p_0(\hat{\beta}_j \mid \mathbf{s}_j)},$$

where  $p_1$  and  $p_0$  denote the marginal likelihoods under the alternative ( $H_1$ ) and null ( $H_0$ ) hypotheses, respectively. Under the null hypothesis,  $H_0$ , we have  $\mathbb{E}_0(\text{BF}_j) = 1$ , regardless of how the alternative hypothesis  $H_1$  is specified.

---

**Algorithm 1** BF-based adjustment of  $\pi_0$ .

---

**Require:** A  $J \times (K + 1)$  matrix  $\mathbf{L}$  in which element  $(j, k)$  is  $\ell_{jk}$ , the marginal likelihood of unit  $j$  under the  $k$ th component of the mixture prior; the estimated prior weights,  $\hat{\boldsymbol{\pi}} = (\hat{\pi}_0, \dots, \hat{\pi}_K) \in \mathbb{R}^{K+1}$ ; a set of candidate cutoff values,  $\mathcal{C} \subset \mathbb{R}^+$  a “buffer” tuning parameter,  $\epsilon > 0$ , typically close to zero.

- 1: Normalize the alternative weights,  $\hat{\pi}_k^* = \hat{\pi}_k / \sum_{k'=1}^K \hat{\pi}'_{k'}, k = 1, \dots, K$ .
- 2: Compute the “collapsed” likelihoods,  $\ell_{j0}^c = \ell_{j0}$  and  $\ell_{j1}^c = \sum_{k=1}^K \ell_{jk} \hat{\pi}_k^*$ ,  $j = 1, \dots, J$ .
- 3: Compute the Bayes factors,  $\text{BF}_j = \ell_{j1}^c / \ell_{j0}^c$  for  $j = 1, \dots, J$ .
- 4: **for**  $c \in \mathcal{C}$  **do**
- 5:    $J_0 = \sum_{j=1}^J \mathbb{I}\{\text{BF}_j < c\}$
- 6:    $\hat{\pi}_0(c) = J_0 / J$ .
- 7:    $\mu(c) = \sum_{j=1}^J \text{BF}_j \times \mathbb{I}\{\text{BF}_j < c\} / J_0$ .
- 8: **end for**
- 9:  $c^* = \inf\{c \in \mathcal{C} : \mu(c) \geq 1 + \epsilon\}$ .
- 10: Adjust the null prior weights,  $\hat{\pi}_0 = \hat{\pi}_0(c^*)$ .
- 11: Adjust the alternative prior weights,  $\hat{\pi}_k = \hat{\pi}_k^*(1 - \hat{\pi}_0(c^*))$ ,  $k = 1, \dots, K$ .
- 12: **return** the adjusted weights,  $\hat{\boldsymbol{\pi}} = (\hat{\pi}_0, \dots, \hat{\pi}_K)$ .

---

*Proof.*

$$\mathbb{E}_0(\text{BF}_j) = \int \frac{p_1(\hat{\boldsymbol{\beta}}_j \mid \mathbf{s}_j)}{p_0(\hat{\boldsymbol{\beta}}_j \mid \mathbf{s}_j)} \times p_0(\hat{\boldsymbol{\beta}}_j \mid \mathbf{s}_j) d\hat{\boldsymbol{\beta}}_j = \int p_1(\hat{\boldsymbol{\beta}}_j \mid \mathbf{s}_j) d\hat{\boldsymbol{\beta}}_j = 1.$$

□

Let  $J_0$  and  $J_1$  denote the numbers of null and alternative units, respectively, with  $J = J_0 + J_1$  and  $\pi_0 = J_0 / J$ . By the law of large numbers, when  $J_0$  is large we have

$$\frac{1}{J_0} \sum_{j \in \mathcal{H}_0} \text{BF}_j \approx 1,$$

where  $\mathcal{H}_0 \subseteq \{1, \dots, J\}$  denotes the null units. This observation motivates a simple conservative procedure to estimate  $J_0$ , and hence  $\pi_0$ : seek the largest possible set of units that

is, on average, consistent with being all null (average  $BF \leq 1$ ). Algorithm 1 implements this procedure, which we call the *BF-based adjustment of  $\pi_0$* . The following Theorem 1 establishes the conservativeness of the adjusted  $\hat{\pi}_0$ .

**Theorem 1** (BF-based adjustment gives conservative estimate). Assume  $\hat{\pi}_0$  is obtained from Algorithm 1, and the  $J_0$  null effects are iid from the null distribution specified by the prior. Then for any alternative distribution, and for any  $\epsilon > 0$ ,

$$\hat{\pi}_0 \geq \pi_0 \text{ almost surely as } J_0 \rightarrow \infty.$$

The proof of this theorem is given in Appendix B of the supplement.

Importantly, *Theorem 1 requires only that the null distribution be correctly specified* (the  $k = 0$  mixture component of the FASH prior,  $g_\beta$ ), whereas the alternative distribution (mixture components 1 through  $K$  in  $g_\beta$ ) may be misspecified. For example, this result does not depend on the shrinkage values  $\sigma_1, \dots, \sigma_K$ , which means that the BF-based adjustment should work even when a coarse grid of values is used to reduce computation.

The requirement that the null hypothesis be correctly specified is analogous to the usual conditions required for calibration of classical  $p$ -values, and is much less onerous than the requirement that the full distribution be correctly specified. Nonetheless, in this setting the requirement is not entirely benign, since the null distribution is not simply a point mass at zero, but rather a diffuse distribution over the function class  $S_0$  of dimension  $p \geq 1$ . (While diffuse priors can be a problem for Bayes factor computation, as they can make the marginal likelihood arbitrarily scaled, here the diffuse component is shared across all mixture components, so these arbitrary scales cancel out when taking their ratio, and the resulting Bayes factors remain valid; see Cheng and Speckman 2016; Servin and Stephens 2007.) If the true null functions are not diffuse over  $S_0$ , then technically this introduces prior misspecification and the conditions of Theorem 1 fail to hold. Nonetheless, in our

experiments the BF-based adjustments produced consistently conservative estimates of  $\hat{\pi}_0$ , even when the prior is misspecified (see Appendix C of the supplement).

From (13) and (15), overestimating  $\hat{\pi}_0$  in the FASH prior shifts posterior mass toward the baseline model,  $S_0$ , yielding more conservative decisions against  $H_0$ . See Figure 2 for an illustration of this. In Appendix B of the supplement, we provide further details by examining the posterior odds comparing the null and the alternative. The conservative behavior of related quantities, such as the lfdr and lfsr, is also investigated empirically in the Appendix C of the supplement.

## 4 Analysis of Dynamic eQTLs in the iPSC Cardiomyocyte Differentiation Study

We evaluated FASH on a variety of performance measures in simulated data sets. These simulation experiments are described in detail in Appendix C of the supplement. Of note, our simulations confirmed that the BF-based adjustment produces conservative estimates of  $\pi_0$ , and therefore produces conservative estimates of lfdr and FDR, even when the prior is misspecified. Reassuringly, these conservative estimates did not substantially reduce power.

Now we focus on a real data application, a reanalysis of dynamic eQTLs in the iPSC cardiomyocyte differentiation study (Strober et al., 2019). This study measured daily gene expression over a 16-day period in induced pluripotent stem cells (iPSCs) derived from 19 Yoruba HapMap cell lines undergoing differentiation into cardiomyocytes. The goals of the analysis were to identify the dynamic eQTLs—that is, to identify genetic loci whose effects on gene expression vary over time—and to characterize how genetic regulation of gene expression changes throughout the process of differentiation. We show that FASH is able to meet these goals in a principled way, and we compare the FASH results to the

original analysis based on parametric interaction models.

After carrying out the data preprocessing and quality control procedures from Strober et al. (2019), we obtained data on  $J = 1,009,173$  gene-variant pairs (6,362 genes). All the genetic variants considered in this analysis were SNPs within 50 kb of the gene’s transcription start site (TSS). For each gene-variant pair  $j \in [J]$ , we obtained eQTL effect estimates  $\hat{\beta}_j(t_r)$  at 16 time points by fitting linear regression models separately for each of the time points  $r \in [16]$ . The standard errors  $s_{jr}$  of the eQTL effect estimates were subsequently adjusted to address concerns about inflation of type I errors due to the small sample size (see Appendix D of the supplement for details).

Specifically, we considered two inference aims:

1. *Identify the dynamic eQTLs.* This was implemented in FASH using mixtures of  $L$ -GP priors with  $L = D^1$ . We refer to the fitted model in this analysis as the “FASH-IWP<sub>1</sub>” model.
2. *Identify the nonlinear dynamic eQTLs.* This was implemented in FASH using mixtures of  $L$ -GP priors with  $L = D^2$ . We refer to the fitted model in this analysis as the “FASH-IWP<sub>2</sub>” model.

All the results were generated using version 0.1.42 of our R package, `fashr`. R code implementing our analyses is available at <https://github.com/stephenslab/fashr-paper>. In all of the analyses, the FASH priors were defined on an equally spaced grid on the log-scale; see Appendix D for details. After estimating the mixture weights  $\pi$  by maximum-likelihood, we applied the BF-based adjustment, then we used the adjusted weights  $\hat{\pi}$  to make inferences from the posterior distributions  $p(\beta_j | \hat{\beta}_j, \mathbf{s}_j, \hat{\pi})$ . We used an FDR threshold of  $\alpha = 0.05$  for identifying “significant” dynamic eQTLs.<sup>1</sup> Performing each of the FASH analyses end-to-end

---

<sup>1</sup>We use FDR so that the FASH analysis is more comparable to the original analysis, but `lfdr` is generally preferred; see Section 5 for further discussion on the use of FDR and FSR vs. `lfsr` and `lfsr` for hypothesis

using `fashr` took about 11 hours. The computations were performed on Linux machines (Scientific Linux 7.4) with Intel Xeon Gold 6248R (“Cascade Lake”) processors and 16 parallel threads.

## 4.1 Discovery of Dynamic eQTLs

Examining in detail some of the dynamic eQTLs identified by FASH with  $L = D^1$  illustrates the variety of dynamics that can be captured by FASH. The examples in the top row of Fig. 3 (A, B) have effects that appear to gradually become stronger over time. In these examples, both the linear interaction ( $G_c \times t$ , where  $G_c$  is the SNP genotype) and quadratic interaction ( $G_c \times t^2$ ) models used in Strober et al. (2019) also provided good fits to the eQTL effects in these examples, and indeed these gene-variant pairs were identified as dynamic eQTLs in Strober et al. (2019). By contrast, the examples in the middle and bottom rows of Fig. 3 (C–F) were identified as dynamic eQTLs by FASH, but they were not identified in the original analysis. Indeed, in all these examples, the linear and quadratic models appear to be a poor fit for the nonlinear dynamics of these eQTLs; for example, in C and D the effect strengthens rather abruptly around day 5, and in E and F the suddenly gets stronger at around day 10. Dynamic eQTLs C and D were very strongly identified by FASH (lfdr of 0.01 or lower) E and F are “borderline” dynamic eQTLs (lfdr > 0.1) with more subtle temporal dynamics. Additional illustrative examples, including examples of gene-variant pairs that FASH did not identify as dynamic eQTLs, are given in Figures S5, S6 and S10 in the supplement.

As a result, given FASH’s ability to capture diverse temporal patterns, FASH identified many more dynamic eQTLs than the original analysis (Figure 4): at an FDR threshold of  $\alpha = 0.05$ , FASH-IWP<sub>1</sub> identified dynamic eQTLs at 9,205 gene-variant pairs (in 1,177 testing in FASH).

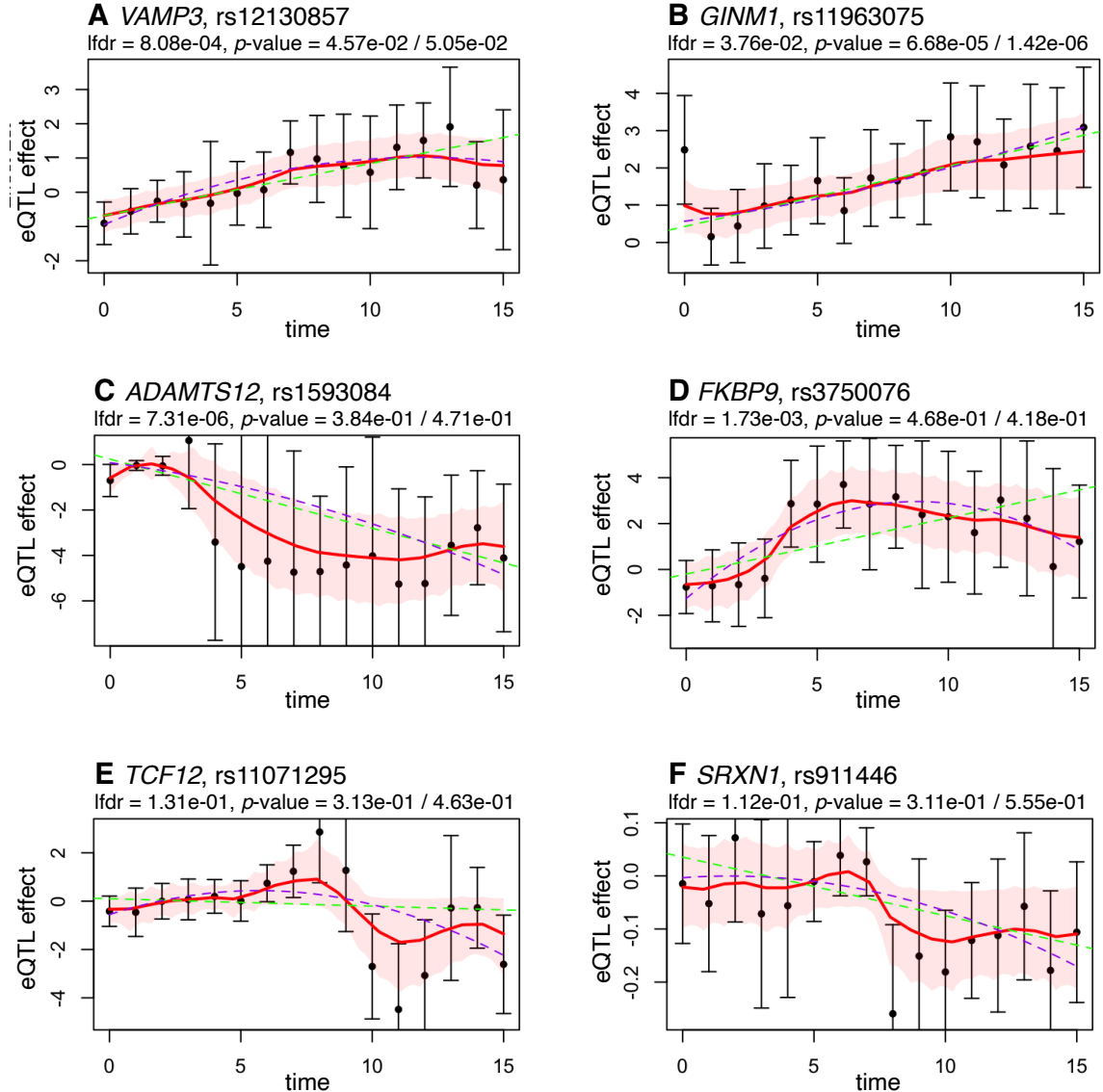


Figure 3: Examples of dynamic eQTLs identified by FASH ( $L = D^1$ ), and comparison with parametric modeling approach (Strober et al., 2019). In each plot, the posterior mean of  $\beta_j$  is shown as a red solid line, and the 95% credible interval is depicted by the shaded region. Observed effect size estimates  $\hat{\beta}_j$  are shown as black dots, with vertical error bars representing  $\pm 2$  the (adjusted) standard errors  $\tilde{s}_{jr}$ . The lfdr is the lfdr from the FASH-IWP<sub>1</sub> model after the BF adjustment; the *p*-values are from the analyses of Strober et al. (2019) with linear/quadratic interaction models. The inverse-variance weighted least squares estimates for the linear ( $G_c \times t$ ) and quadratic ( $G_c \times t^2$ ) parametric interaction models are shown as dashed lines (green = linear, purple = quadratic).

genes), or about 1% of all gene-variant pairs tested (19% of all genes); at an eFDR threshold of 0.05, Strober et al. (2019) identified dynamic eQTLs at 5,404 gene-variant pairs (in 550 genes) using the linear interaction model, and 6824 gene-variant pairs (693 genes) using

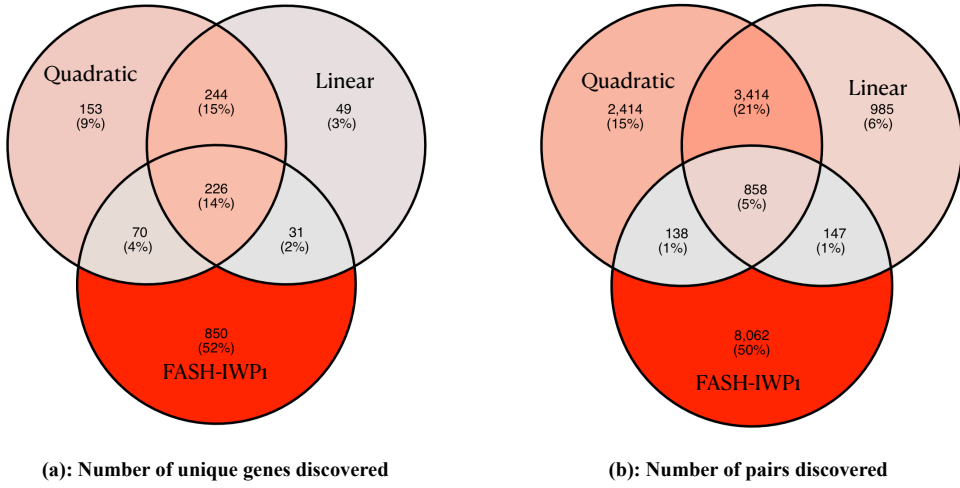


Figure 4: Discovery of dynamic eQTLs using FASH vs. linear/quadratic parametric interaction models: (a) genes and (b) gene-variant pairs.

the quadratic interaction model. Despite the increased discovery of dynamic eQTLs, the FASH inferences are still “conservative” in that they were obtained using the BF-based adjustment of the FASH prior. (The effect of this adjustment on the FASH priors was shown in Figure 2.)

It should be noted that, since there were several other differences in the two analyses beyond the increased flexibility of FASH, it is likely that these differences also contributed to differences in discovery, and may partly explain why many of the dynamic eQTLs identified by the linear and quadratic interaction models were not reproduced in our analysis. For example, recognizing that the small sample sizes may lead to inflated type I errors, we adjusted the standard errors following a simple procedure described in the supplement, whereas the original analysis did not account for this issue. So it is possible that not accounting for this issue in the original analysis lead to a greater number of false positives. Another important consideration is that the two analyses took very different approaches to estimating the false discovery rate: FASH, by taking an empirical Bayes approach, estimates the (prior) null proportion as part of the model fitting, which is then used for the lfdr and FDR estimation; the analysis of Strober et al. (2019) used a permutation-based approach

to estimate the null distribution of  $p$ -values, then applied the approach of Gamazon et al. (2013) to estimate the FDR. See Figures S8 and S9 in the supplement for more detailed comparisons of the two analyses, comparing the FASH lfdr values (and their corresponding FDR estimates) with the  $p$ -values (and the corresponding eFDR estimates) from the original analysis.

## 4.2 Characterization of Dynamic eQTLs

Now we move from discovery of dynamic eQTLs to characterizing the dynamic changes of the dynamic eQTLs; in particular, we would like to characterize *how* the genetic effects on gene expression evolve throughout the process of cell differentiation. Strober et al. (2019) also sought to characterize the dynamic eQTLs, but their statistical analysis was complicated by the limitations of the available methods. Here we show that this is much more straightforwardly accomplished within the FASH modeling framework, as well as being more valid because it is accompanied by (appropriately calibrated) posterior statistics such as lfdrs and lfsrs.

By reanalyzing the data with a linear baseline model instead of a constant baseline model—that is, using a FASH prior with  $L = D^2$ —FASH identifies the gene-variant pairs with *nonlinear* dynamic effects on gene expression. At an FDR threshold of  $\alpha = 0.05$ , this “FASH-IWP<sub>2</sub>” model found a small number nonlinear dynamic eQTLs: 44 gene-variant pairs within 9 genes (Table Table 1). (Without the BF-based adjustment, FASH-IWP<sub>2</sub> identified 159 gene-variant pairs within 37 genes at  $\alpha = 0.05$ , still a much smaller number than the overall number of genes with dynamic eQTLs; see Figure 4.)

A few examples of these nonlinear dynamic eQTLs are shown in Figure 5. (See also Figure S7 for examples of dynamic eQTLs that were not classified as “nonlinear”.) The diversity of the nonlinear effects is quite striking. Clearly, the quadratic interaction model, even though

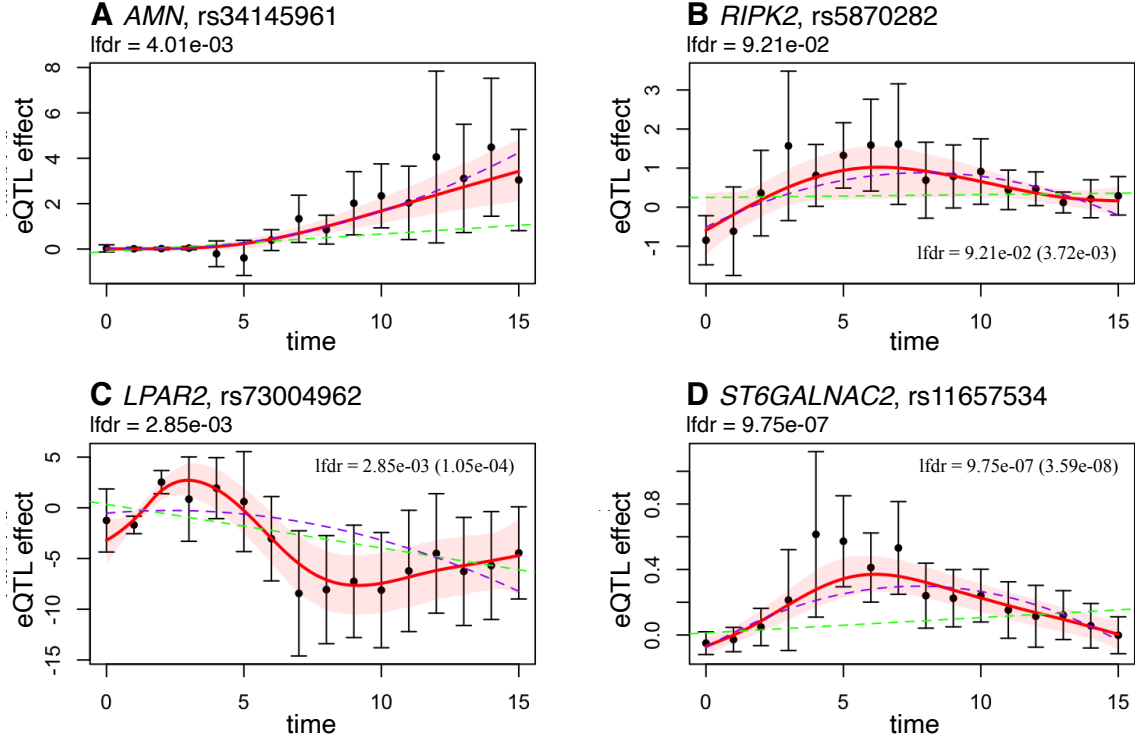


Figure 5: Examples of nonlinear dynamic eQTLs identified by FASH, with  $L = D^2$ . In each plot, the posterior mean of  $\beta_j$  is shown as a red solid line, and the 95% credible interval is depicted by the shaded region. Observed effect size estimates  $\hat{\beta}_j$  are shown as black dots, with vertical error bars representing  $\pm 2$  the (adjusted) standard errors  $\tilde{s}_{jr}$ . The Ifdr is the Ifdr from the FASH-IWP<sub>2</sub> model after the BF adjustment. The inverse-variance weighted least squares estimates for the linear ( $G_c \times t$ ) and quadratic ( $G_c \times t^2$ ) parametric interaction models are shown as dashed lines (green = linear, purple = quadratic).

it was intended for identifying nonlinear dynamic effects in Strober et al. (2019), is not flexible enough to capture the full range of nonlinear effects.

The ability of FASH to test hypotheses of the form  $\mathcal{F}(\beta) = 0$  or  $\mathcal{F}(\beta) > 0$  (Section 3.5.1) for an arbitrary functional  $\mathcal{F}$  provides new ways to characterize dynamic effects in a systematic fashion. For example, Strober et al. (2019) were interested in identifying the dynamic eQTLs with effects on expression that switch direction. To frame this as a hypothesis test, we define a functional  $\mathcal{F}(\beta)$  that measures whether the genotype effect exhibits a sign-changing “switch” with magnitude exceeding a threshold  $c > 0$ :

$$\mathcal{F}(\beta) = \min \left\{ \max_t \beta^+(t), \max_t \beta^-(t) \right\} - c, \quad (19)$$

category	gene-variants	genes	functional, $\mathcal{F}(\beta)$
dynamic	44	9	(not applicable)
early	124	8	$\max_{t \leq 3}  \beta(t)  - \max_{t > 3}  \beta(t) $
middle	24	5	$\max_{4 \leq t \leq 11}  \beta(t)  - \max_{t < 4 \text{ or } t > 11}  \beta(t) $
late	20	12	$\max_{t \geq 12}  \beta(t)  - \max_{t < 12}  \beta(t) $
switch	984	250	$\min\{\max_{0 \leq t \leq 15} \beta^+(t), \max_{0 \leq t \leq 15} \beta^-(t)\} - c, c = 0.25$

Table 1: Classification of dynamic eQTLs based on temporal effect patterns: number of gene-variant pairs and unique genes identified at an FDR (top row) or FSR (other rows) of 0.05. For the *switch* category, setting  $c = 0.25$  ensures that the largest effect size difference across the range of genotype dosages (0–2) is at least 1, since  $2 \times c \times 2 = 1$ . See Figure 6 for examples illustrating each category.

Hallmark gene set	genes	<i>p</i> -value	<i>q</i> -value
	all/switch	all/switch	all/switch
genes up-regulated in response to hypoxia	25/11	0.017/0.00067	0.436/0.025
genes up-regulated by KRAS activation	11/7	0.24/0.0022	0.840/0.035

Table 2: Gene set enrichment analysis of genes with dynamic eQTLs vs. genes with switch dynamic eQTLs. The “genes” column gives the number of dynamic genes eQTL or switch dynamic eQTL genes belonging to the Hallmark gene set (Liberzon et al., 2015a,b; Subramanian et al., 2005). GSEA *p*-values and *q*-values were computed using the “enricher” function in the clusterProfiler R package (Wu et al., 2021; Yu et al., 2012). See Table 3 of the supplement for more detailed GSEA results.

where  $\beta^+$  and  $\beta^-$  denote the positive and negative parts of  $\beta$ , respectively, so that  $\beta = \beta^+ - \beta^-$ . When  $\mathcal{F}(\beta) > 0$ , there exist time points  $t_+$  and  $t_-$  such that  $\beta(t_+) > c$  and  $\beta(t_-) < -c$ , implying an effect difference of at least  $2c$  between these time points for a one-allele change in genotype. For  $c = 0.25$ , this corresponds to a minimum difference of  $4c = 1$  between the two-homozygote genotypes.

In addition to the *switch* category, we used the hypothesis testing framework to group the

dynamic eQTLs into three other categories:

- *Early*: The strongest effect occurs sometime during the first 3 days of cell differentiation.
- *Middle*: The strongest effect occurs sometime between days 4 and 11.
- *Late*: The strongest effect occurs sometime during the final 4 days.

Each of these categories corresponds to an inequality of the form  $\mathcal{F}(\beta) > 0$  (Table 1). (Note that the switch category is not exclusive of the other categories; for example, a dynamic eQTL should be identified as both *early* and *switch*.) The numbers of gene-variants and genes assigned to each of these categories at an FSR threshold of 0.05 (after applying the BF-based adjustment to the prior) are given in Table 1. Examples of dynamic eQTLs in each category are shown in Figure 6. Only a very small number of dynamic eQTLs were classified *early*, *middle* or *late*, but many dynamic eQTLs were identified as having effects that switch direction. To better understand the biological significance of the switch dynamic eQTLs, we performed a gene set enrichment analysis (GSEA) on the Hallmark gene sets (Liberzon et al., 2015a,b; Subramanian et al., 2005) using clusterProfiler (Wu et al., 2021; Yu et al., 2012), and compared the GSEA results for the 250 genes with switch dynamic eQTLs vs. the 1,177 genes with any type of dynamic eQTL. Interestingly, the top two Hallmark gene sets for the switch dynamic eQTLs (ranked by *p*-value) were genes upregulated in low oxygen levels (i.e., hypoxia) and genes upregulated by K-Ras, and these were also among the top gene sets for all dynamic eQTLs, but the enrichments were much stronger when considering the switch dynamic eQTLs only (Table 2). Both hypoxia and K-Ras are well known to have strong effects on proliferation and differentiation of stem cells, and so it potentially significant that the switch dynamic eQTLs are more strongly enriched for these pathways. More detailed GSEA results are provided in Table 3 in the supplement.

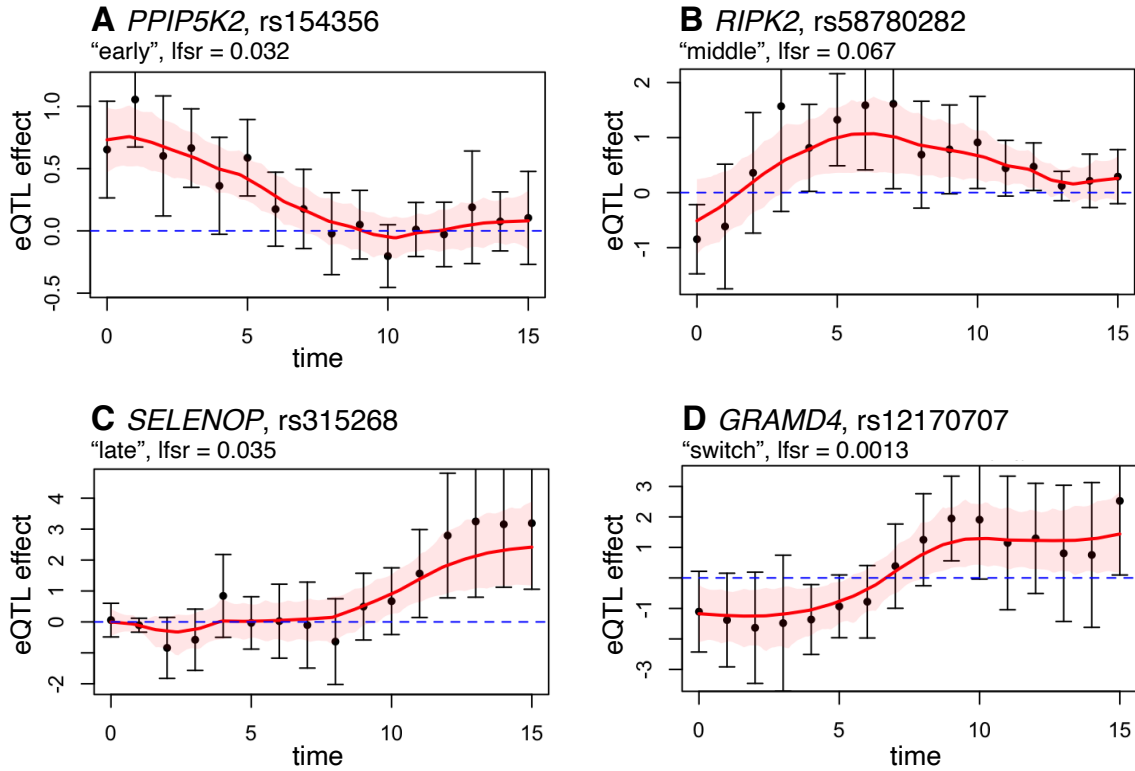


Figure 6: Examples of dynamic eQTLs categorized by FASH as being (A) *early*, (B) *middle*, (C) *late* and (D) *switch*. (See Table 1 for definitions of these categories.) The posterior mean of  $\beta_j$  is shown as a red solid line, and the 95% credible interval is depicted by the shaded region. Observed effect size estimates  $\hat{\beta}_j$  are shown as black dots, with vertical error bars representing  $\pm 2$  the (adjusted) standard errors  $\tilde{s}_{jr}$ . “lfsr” is the lfsr obtained using the BF-adjusted prior.

## 5 Discussion

In this paper, we extended empirical Bayes (EB) ideas to reason about posterior distributions on *functions*. This resulted in a powerful and flexible modeling framework, FASH (“functional adaptive shrinkage”), that can be used to test various hypotheses about functions. FASH automatically adapts the priors by borrowing information across all observation units, so the posterior inferences should become more accurate as more data becomes available. In the case study, where we used FASH to reanalyze dynamic eQTLs, a particularly appealing aspect of FASH was being able to categorize the dynamic eQTLs into different types (Table 1).

We also proposed a simple adjustment to the prior to address concerns about miscalibration

of the FDR and other posterior statistics when the prior is misspecified. This adjustment results in more conservative estimates of the prior—that is, greater weight on the null proportion,  $\pi_0$ —and therefore it is more conservative in its inferences. This proposal is not specific to FASH, and therefore could potentially be used in other EB methods, particularly in high-dimensional multivariate data settings (Urbut et al., 2019; Liu et al., 2024) where prior misspecification is likely to occur.

Although FASH defines posterior distributions on *functions*, the actual computations involve probability distributions on finite-dimensional spaces, making the computations tractable. To make these tractable posterior computations scalable to large data sets, we chose the “*L*-GP” family of priors because they produce posterior computations with complexity that scales linearly in  $J$ , the number of observation units, and  $R_j$ , the number of observations per unit; more details on the complexity of the posterior computations are given in Appendix A of the supplement (The posterior computations with standard GPs scale cubically in  $R_j$ ). Beyond computationally efficiency, the “*L*-GP” family also provides flexibility in hypothesis testing. In principle, FASH could be extended to other GP prior families, motivated by other applications. For example, prior families based on spatial Gaussian random fields (Lindgren et al., 2011) could be of interest applications involving spatial data.

Similar to studying the genetic effects on gene expression over time (“dynamic eQTLs”), there is also considerable interest in using single-cell RNA-sequencing (Stegle et al., 2015) to study how eQTL effects vary along continuous cellular contexts such as cell differentiation trajectories (van der Wijst et al., 2020). A FASH analysis of such data could involve mapping the cells onto a 1-d trajectory, then applying FASH to the effects estimated at the different points along the trajectory.

Finally, a practical point regarding FASH is that local significance measures, such as lfsr and lfsr, are usually preferred over cumulative significance measures such as FDR and FSR.

We have found that when many of the observations have local measures close to zero, this can have the effect of pulling down the cumulative average over all the observation units, resulting in small FDR (or FSR), even when the lfdr (or lfsr) is large. In situations such as this, using the local significance measures will reduce false discoveries compared to the cumulative significance measures.

## 6 Disclosure Statement

The authors have no conflicts of interest to report.

## 7 Data Availability Statement

The summary statistics used in the dynamic eQTL analysis are provided in the online supplementary material, and the code to replicate the result is available on Github.

## 8 Acknowledgments

The authors thank Kenneth Barr for his support with the cardiomyocyte data analyzed in Section 4.

## 9 Funding

This research was supported in part by grants from the NSF (DMS-2235451) and Simons Foundation (MPS-NITMB-00005320) to the NSF-Simons National Institute for Theory and Mathematics in Biology (NITMB).

## SUPPLEMENTARY MATERIAL

**Supplementary Text and Figures:** Additional proofs and derivations, evaluation of FASH on simulated data sets, FASH implementation details, and supplementary figures. (PDF file)

**Supplementary Data:** Summary statistics of eQTL effect estimates for all gene–variant pairs across all time points, as analyzed in Section 4. (ZIP file)

## References

Benjamini, Y. and Hochberg, Y. (1995). Controlling the false discovery rate: a practical and powerful approach to multiple testing. *Journal of the Royal Statistical Society, Series B*, 57(1):289–300.

Cheng, C.-I. and Speckman, P. L. (2016). Bayes factors for smoothing spline ANOVA. *Bayesian Analysis*, 11(4):957–975.

Cuomo, A. S., Seaton, D. D., McCarthy, D. J., Martinez, I., Bonder, M. J., Garcia-Bernardo, J., Amatya, S., Madrigal, P., Isaacson, A., Buettner, F., et al. (2020). Single-cell RNA-sequencing of differentiating iPS cells reveals dynamic genetic effects on gene expression. *Nature Communications*, 11:810.

DeRisi, J. L., Iyer, V. R., and Brown, P. O. (1997). Exploring the metabolic and genetic control of gene expression on a genomic scale. *Science*, 278(5338):680–686.

Efron, B. (2008). Microarrays, empirical Bayes and the two-groups model. *Statistical Science*, 23(1):1–22.

Efron, B. (2009). Empirical Bayes estimates for large-scale prediction problems. *Journal of the American Statistical Association*, 104(487):1015–1028.

Elorbany, R., Popp, J. M., Rhodes, K., Strober, B. J., Barr, K., Qi, G., Gilad, Y., and Battle, A. (2022). Single-cell sequencing reveals lineage-specific dynamic genetic regulation of gene expression during human cardiomyocyte differentiation. *PLoS Genetics*, 18(1):e1009666.

Francesconi, M. and Lehner, B. (2014). The effects of genetic variation on gene expression dynamics during development. *Nature*, 505(7482):208–211.

Gamazon, E. R., Huang, R. S., Dolan, M. E., Cox, N. J., and Im, H. K. (2013). Integrative genomics: quantifying significance of phenotype-genotype relationships from multiple sources of high-throughput data. *Frontiers in Genetics*, 3.

Gutierrez-Arcelus, M., Baglaenko, Y., Arora, J., Hannes, S., Luo, Y., Amariuta, T., et al. (2020). Allele-specific expression changes dynamically during T cell activation in HLA and other autoimmune loci. *Nature Genetics*, 52(3):247–253.

Heller, R. A., Schena, M., Chai, A., Shalon, D., Bedilion, T., Gilmore, J., Woolley, D. E., and Davis, R. W. (1997). Discovery and analysis of inflammatory disease-related genes using cdna microarrays. *Proceedings of the National Academy of Sciences*, 94(6):2150–2155.

Hughes, T. R., Marton, M. J., Jones, A. R., Roberts, C. J., Stoughton, R., Armour, C. D., et al. (2000). Functional discovery via a compendium of expression profiles. *Cell*, 102(1):109–126.

Kang, J. B., Shen, A. Z., Gurajala, S., Nathan, A., Rumker, L., Aguiar, V. R. C., et al. (2023). Mapping the dynamic genetic regulatory architecture of HLA genes at single-cell resolution. *Nature Genetics*, 55(12):2255–2268.

Kim, Y., Carbonetto, P., Stephens, M., and Anitescu, M. (2020). A fast algorithm for maximum likelihood estimation of mixture proportions using sequential quadratic programming. *Journal of Computational and Graphical Statistics*, 29(2):261–273.

Li, G. H., Shi, Y., Chen, Y., Sun, M., Sader, S., Maekawa, Y., et al. (2009). Gelsolin regulates cardiac remodeling after myocardial infarction through DNase I-mediated apoptosis. *Circulation Research*, 104(7):896–904.

Liberzon, A., Birger, C., Thorvaldsdóttir, H., Ghandi, M., Mesirov, J. P., and Tamayo, P.

(2015a). The Molecular Signatures Database hallmark gene set collection. *Cell Systems*, 1(6):417–425.

Liberzon, A., Birger, C., Thorvaldsdóttir, H., Ghandi, M., Mesirov, J. P., and Tamayo, P. (2015b). The molecular signatures database hallmark gene set collection. *Cell Systems*, 1(6):417–425.

Lindgren, F. and Rue, H. (2008). On the second-order random walk model for irregular locations. *Scandinavian Journal of Statistics*, 35(4):691–700.

Lindgren, F., Rue, H., and Lindström, J. (2011). An explicit link between gaussian fields and gaussian markov random fields: the stochastic partial differential equation approach. *Journal of the Royal Statistical Society Series B: Statistical Methodology*, 73(4):423–498.

Liu, Y., Carbonetto, P., Takahama, M., Gruenbaum, A., Xie, D., Chevrier, N., and Stephens, M. (2024). A flexible model for correlated count data, with application to multicondition differential expression analyses of single-cell RNA sequencing data. *Annals of Applied Statistics*, 18(3):2551–2575.

Lu, M. and Stephens, M. (2019). Empirical Bayes estimation of normal means, accounting for uncertainty in estimated standard errors. *arXiv*, 1901.10679.

MacKay, D. J. (2003). *Information Theory, Inference, and Learning Algorithms*. Cambridge University Press.

Mazzotta, S., Neves, C., Bonner, R. J., Bernardo, A. S., Docherty, K., and Hoppler, S. (2016). Distinctive roles of canonical and noncanonical Wnt signaling in human embryonic cardiomyocyte development. *Stem Cell Reports*, 7(4):764–776.

Nathan, A., Asgari, S., Ishigaki, K., Valencia, C., Amariuta, T., Luo, Y., et al. (2022). Single-cell eQTL models reveal dynamic T cell state dependence of disease loci. *Nature*, 606(7912):120–128.

Polson, N. G. and Scott, J. G. (2010). Shrink globally, act locally: sparse Bayesian regularization and prediction. *Bayesian Statistics*, 9.

Särkkä, S. and Solin, A. (2019). *Applied stochastic differential equations*, volume 10. Cambridge University Press, Cambridge, UK.

Servin, B. and Stephens, M. (2007). Imputation-based analysis of association studies: candidate regions and quantitative traits. *PLoS Genetics*, 3(7):e114.

Shepp, L. A. (1966). Radon-Nikodym derivatives of Gaussian measures. *Annals of Mathematical Statistics*, pages 321–354.

Soskic, B., Cano-Gamez, E., Smyth, D. J., Ambridge, K., Ke, Z., Matte, J. C., et al. (2022). Immune disease risk variants regulate gene expression dynamics during cd4+ t cell activation. *Nature Genetics*, 54(6):817–826.

Stegle, O., Teichmann, S. A., and Marioni, J. C. (2015). Computational and analytical challenges in single-cell transcriptomics. *Nature Reviews Genetics*, 16(3):133–145.

Stephens, M. (2017). False discovery rates: a new deal. *Biostatistics*, 18(2):275–294.

Storey, J. D. (2002). A direct approach to false discovery rates. *Journal of the Royal Statistical Society, Series B*, 64(3):479–498.

Strober, B., Elorbany, R., Rhodes, K., Krishnan, N., Tayeb, K., Battle, A., and Gilad, Y. (2019). Dynamic genetic regulation of gene expression during cellular differentiation. *Science*, 364(6447):1287–1290.

Subramanian, A., Tamayo, P., Mootha, V. K., Mukherjee, S., Ebert, B. L., Gillette, M. A., Paulovich, A., Pomeroy, S. L., Golub, T. R., Lander, E. S., and Mesirov, J. P. (2005). Gene set enrichment analysis: a knowledge-based approach for interpreting genome-wide expression profiles. *Proceedings of the National Academy of Sciences*, 102(43):15545–15550.

Urbut, S. M., Wang, G., Carbonetto, P., and Stephens, M. (2019). Flexible statistical

methods for estimating and testing effects in genomic studies with multiple conditions.

*Nature Genetics*, 51:187–195.

van der Wijst, M. G., de Vries, D. H., Groot, H. E., Trynka, G., Hon, C.-C., Bonder, M.,

Stegle, O., Nawijn, M., Idaghdour, Y., Van Der Harst, P., et al. (2020). The single-cell eqtlgen consortium. *elife*, 9:e52155.

Vovk, V. and Wang, R. (2021). E-values: calibration, combination and applications. *Annals of Statistics*, 49(3):1736–1754.

Wahba, G. (1978). Improper priors, spline smoothing and the problem of guarding against model errors in regression. *Journal of the Royal Statistical Society, Series B*, 40(3):364–372.

Willwerscheid, J., Carbonetto, P., and Stephens, M. (2025). ebnm: an R package for solving the empirical Bayes normal means problem using a variety of prior families. *Journal of Statistical Software*, 114(3):1–32.

Wu, T., Hu, E., Xu, S., Chen, M., Guo, P., Dai, Z., Feng, T., Zhou, L., Tang, W., Zhan, L., Fu, X., Liu, S., Bo, X., and Yu, G. (2021). clusterprofiler 4.0: a universal enrichment tool for interpreting omics data. *The Innovation*, 2(3):100141.

Yu, G., Wang, L.-G., Han, Y., and He, Q.-Y. (2012). clusterProfiler: an R package for comparing biological themes among gene clusters. *OMICS: A Journal of Integrative Biology*, 16(5):284–287.

Yue, Y. R., Simpson, D., Lindgren, F., and Rue, H. (2014). Bayesian adaptive smoothing splines using stochastic differential equations. *Bayesian Analysis*, 9(2):397–424.

Zhang, Z., Brown, P., and Stafford, J. (2025). Efficient modeling of quasi-periodic data with seasonal Gaussian process. *Statistics and Computing*, 35:32.

Zhang, Z., Stringer, A., Brown, P., and Stafford, J. (2024). Model-based smoothing with Integrated Wiener Processes and overlapping splines. *Journal of Computational and Graphical Statistics*, 33(3):883–895.

# Empirical Bayes Shrinkage of Functional Effects, with Application to Analysis of Dynamic eQTLs: Supplementary Text and Figures

Ziang Zhang, Peter Carbonetto and Matthew Stephens

## Appendix A: Implementation Details

This section provides additional details on the implementation of FASH across its main computational steps.

### Choice of the Grid for $\sigma_k$

We fix  $\sigma_0 = 0$  to represent the null component, and construct the remaining  $K$  grid values  $\{\sigma_k\}_{k=1}^K$  following the strategy in Stephens (2017). The goal is to create a sufficiently dense grid covering the interval  $[\sigma_{\min}, \sigma_{\max}]$ , such that the inferential results remain stable and do not change noticeably when using a larger or denser grid.

Conceptually,  $\sigma_k$  controls the deviation from the baseline model  $S_0$ . Its interpretation in practice depends on the choice of operator  $L$  defining the  $L$ -GP, as well as the measurement scale. To provide a more interpretable and consistent scale across applications, we consider an equivalent reparameterization in terms of the  $h$ -unit predictive standard deviation (PSD) (Zhang et al., 2024, 2025), defined as

$$\sigma(h) = \text{SD}[\beta(t+h) \mid \beta(s) : s \leq t], \quad \beta \sim L\text{-GP}(\beta; \sigma). \quad (20)$$

The PSD  $\sigma(h)$  is a positive scaling of the original  $\sigma$ , but has a direct interpretation in terms of function variability that is comparable across different choices of  $L$ .

By default, we choose  $[\sigma_{\min}, \sigma_{\max}]$  based on the one-unit PSD  $\sigma(1)$ , with grid values  $\{\sigma_k\}_{k=1}^K$  equally spaced in log-precision scale, i.e.  $-2 \log \sigma_k(1)$  between 0 and 10. While other settings

can be explored, this default has been found to perform well in our experience.

## Computing the Likelihood Matrix $\mathbf{L}$

The main computational step of FASH is the evaluation of the likelihood matrix  $\mathbf{L} \in \mathbb{R}^{J \times (K+1)}$ . For each entry,

$$\begin{aligned}\mathbf{L}_{jk} &= p_k(\hat{\boldsymbol{\beta}}_j \mid \mathbf{s}_j) \\ &= \int p(\hat{\boldsymbol{\beta}}_j \mid \boldsymbol{\beta}_j, \mathbf{s}_j) p(\boldsymbol{\beta}_j \mid \sigma_k) d\boldsymbol{\beta}_j \\ &= d\mathcal{N}(\hat{\boldsymbol{\beta}}_j; \mathbf{0}, \mathbf{C}_k + \mathbf{S}_j),\end{aligned}\tag{21}$$

where  $\mathbf{C}_k$  is the covariance of  $\boldsymbol{\beta}_j$  under  $\beta_j \sim L\text{-GP}(\beta_j; \sigma_k)$  and  $\mathbf{S}_j$  is a diagonal matrix of squared standard errors.

Evaluating Equation (21) requires the precision matrix  $(\mathbf{C}_k + \mathbf{S}_j)^{-1}$ . When  $R_j$  is large, direct inversion becomes computationally expensive, with  $O(R_j^3)$  time and  $O(R_j^2)$  memory. However, unlike standard GPs, the  $L$ -GP has a Markovian structure due to its construction from differential operators (Särkkä and Solin, 2019), which can be exploited to reduce computational complexity to  $O(R_j)$ . This can be achieved either by augmenting  $\boldsymbol{\beta}_j$  with its derivatives, or by finite element approximation (Lindgren and Rue, 2008; Zhang et al., 2024, 2025). In this work, we adopt the latter approach using 20 equally spaced O-splines as the default.

## Optimizing the Empirical Bayes Prior $\hat{g}_\beta$

The empirical Bayes (EB) estimate  $\hat{g}_\beta$  is obtained by maximizing the log-likelihood in Equation (11). To encourage conservative estimation of  $\pi_0$ , a Dirichlet-based penalty can be added (Stephens, 2017):

$$h(\boldsymbol{\pi}; \lambda) = \prod_{k=0}^K \pi_k^{\lambda_k - 1}, \quad \lambda_k \geq 1,\tag{22}$$

yielding the penalized log-likelihood

$$l(\boldsymbol{\pi}) + \log h(\boldsymbol{\pi}) = \sum_{j=1}^J \log \left( \sum_{k=0}^K \pi_k \mathbf{L}_{jk} \right) + \sum_{k=0}^K (\lambda_k - 1) \log \pi_k. \quad (23)$$

This convex optimization problem can be solved efficiently with constrained algorithms; we use the sequential quadratic programming method of Kim et al. (2020) with  $\lambda_0 = 10$  and  $\lambda_k = 1$  for  $k \neq 0$ .

Although Equation (23) assumes independence across units, in the presence of dependence it can be interpreted as a composite likelihood, and the EB estimate  $\hat{\boldsymbol{\pi}}$  typically remains consistent (Urbut et al., 2019).

## Posterior Computation

Given  $\mathbf{L}$  and  $\hat{g}_\beta$ , the posterior for each  $\beta_j$  is obtained as the mixture in Equation (12). Each component posterior  $p_k(\beta_j | \hat{\boldsymbol{\beta}}, \mathbf{s})$  is a GP, so the overall posterior is a mixture of  $K + 1$  GPs. In practice,  $\hat{\boldsymbol{\pi}}$  is typically sparse, so that only a few non-trivial mixture components remain, reducing the memory required to store posterior processes.

To compute lfsr in Equation (17) for a functional  $\mathcal{F}$ , we draw  $M$  independent sample paths from the non-trivial components of the posterior mixture and approximate the relevant probabilities via Monte Carlo. The finite element representation of the LGP makes path simulation computationally efficient even for large  $M$ ; we use  $M = 3000$  by default in our analysis.

## Appendix B: Additional proofs and derivations

### Proof of Theorem 1

**Theorem 1** (BF-adjustment gives conservative estimate). *Assume  $\hat{\pi}_0$  is the adjusted estimate of  $\pi_0 = J_0/J$  obtained from Algorithm 1, and that the  $J_0$  null effects are i.i.d. from the null distribution specified in the adaptive prior. Then for any specification of the alternative distributions (components 1 to  $K$ ) in the prior and any buffer  $\epsilon > 0$ ,*

$$\hat{\pi}_0 \geq \pi_0 \quad \text{almost surely as } J_0 \rightarrow \infty.$$

*Proof.* By Lemma 1, under the null  $\mathbb{E}_0(\text{BF}_j) = 1$  and  $\text{BF}_j > 0$ . Hence, by the strong law of large numbers,

$$\lim_{J_0 \rightarrow \infty} \frac{1}{J_0} \sum_{j \in \mathcal{H}_0} \text{BF}_j = 1 \quad \text{almost surely.} \quad (24)$$

From now on, all asymptotic arguments are understood almost surely, so we omit the notation.

Define the thresholded sets induced by  $c^*$ :

$$\mathcal{T}_0 = \{j : \text{BF}_j < c^*\}, \quad \mathcal{T}_1 = \{j : \text{BF}_j \geq c^*\}.$$

Let  $J_{a,b} = |\mathcal{H}_a \cap \mathcal{T}_b|$  for  $a, b \in \{0, 1\}$ , and set

$$S = \sum_{j \in \mathcal{H}_0 \cap \mathcal{T}_0} \text{BF}_j.$$

Then  $J_{0,0} + J_{0,1} = J_0$ , and

$$\hat{\pi}_0 = \frac{J_{0,0} + J_{1,0}}{J}, \quad \pi_0 = \frac{J_{0,0} + J_{0,1}}{J}. \quad (25)$$

Thus proving  $\hat{\pi}_0 \geq \pi_0$  is equivalent to showing  $J_{1,0} \geq J_{0,1}$ .

By (24), there exists a positive integer  $J'_0$  such that for all  $J_0 > J'_0$ ,

$$1 + \frac{\epsilon}{2} \geq \frac{\sum_{j \in \mathcal{H}_0} \text{BF}_j}{J_0} = \frac{\sum_{j \in \mathcal{H}_0 \cap \mathcal{T}_1} \text{BF}_j + S}{J_{0,1} + J_{0,0}} \geq \frac{c^* J_{0,1} + S}{J_{0,1} + J_{0,0}}, \quad (26)$$

where the last inequality holds since  $\text{BF}_j \geq c^*$  on  $\mathcal{T}_1$ .

By the definition of  $c^*$  in Algorithm 1, we have  $\mu(c^*) \geq 1 + \epsilon$ , hence

$$1 + \frac{\epsilon}{2} \leq \mu(c^*) = \frac{\sum_{j \in \mathcal{T}_0} \text{BF}_j}{J_{1,0} + J_{0,0}} = \frac{\sum_{j \in \mathcal{H}_1 \cap \mathcal{T}_0} \text{BF}_j + S}{J_{1,0} + J_{0,0}} \leq \frac{c^* J_{1,0} + S}{J_{1,0} + J_{0,0}}, \quad (27)$$

where the last inequality holds since  $\text{BF}_j < c^*$  on  $\mathcal{T}_0$ .

Combining (26) and (27), for all large enough  $J_0$ ,

$$\frac{c^* J_{0,1} + S}{J_{0,1} + J_{0,0}} \leq 1 + \frac{\epsilon}{2} \leq \frac{c^* J_{1,0} + S}{J_{1,0} + J_{0,0}}. \quad (28)$$

Define

$$f(x) = \frac{c^* x + S}{x + J_{0,0}}, \quad f'(x) = \frac{c^* J_{0,0} - S}{(x + J_{0,0})^2}.$$

Since  $\text{BF}_j < c^*$  on  $\mathcal{T}_0$ , we have  $S < c^* J_{0,0}$ . Therefore,  $f'(x) > 0$  for  $x > 0$ , so  $f$  is strictly increasing. From (28),  $f(J_{0,1}) \leq f(J_{1,0})$ , which implies  $J_{1,0} \geq J_{0,1}$ .

Finally, by (25), this yields  $\hat{\pi}_0 \geq \pi_0$ , completing the proof.  $\square$

## Conservativeness of posterior odds

In this subsection, we give additional details showing that overestimating  $\pi_0$  makes inference more conservative in favor of  $H_0$ , even when the alternative is misspecified.

For simplicity, assume  $\tilde{\pi}_0$  is fixed with  $0 < \pi_0 \leq \tilde{\pi}_0 < 1$ , and denote

$$p_0 = p_0(\hat{\beta}_j \mid \mathbf{s}_j), \quad p_1 = p_1(\hat{\beta}_j \mid \mathbf{s}_j), \quad \tilde{p}_1 = \tilde{p}_1(\hat{\beta}_j \mid \mathbf{s}_j),$$

as the null, true alternative, and misspecified alternative marginal densities, respectively.

A useful measure of the evidence against  $H_0$  is the *posterior odds* (PO), defined by

$$\text{PO} = \frac{p(H_1 \mid \hat{\beta}_j, \mathbf{s}_j)}{p(H_0 \mid \hat{\beta}_j, \mathbf{s}_j)} = \frac{1 - \pi_0}{\pi_0} \frac{p_1}{p_0}. \quad (29)$$

Replacing  $\pi_0$  and  $p_1$  by their adjusted/misspecified counterparts yields the fitted  $\widetilde{\text{PO}}$ :

$$\widetilde{\text{PO}} = \frac{1 - \tilde{\pi}_0}{\tilde{\pi}_0} \frac{\tilde{p}_1}{p_0}. \quad (30)$$

First, it is straightforward to show, under the null, the fitted  $\widetilde{\text{PO}}$  is more conservative than the true  $\text{PO}$  in expectation:

**Lemma S1:** *If  $\tilde{\pi}_0 \geq \pi_0$ , then*

$$\mathbb{E}_{H_0}[\widetilde{\text{PO}}] \leq \mathbb{E}_{H_0}[\text{PO}].$$

*Proof.* From (29)-(30) and taking expectation with respect to  $p_0$ ,

$$\mathbb{E}_{H_0}[\widetilde{\text{PO}}] = \frac{1 - \tilde{\pi}_0}{\tilde{\pi}_0} \mathbb{E}_{p_0} \left[ \frac{\tilde{p}_1}{p_0} \right] = \frac{1 - \tilde{\pi}_0}{\tilde{\pi}_0}, \quad \mathbb{E}_{H_0}[\text{PO}] = \frac{1 - \pi_0}{\pi_0} \mathbb{E}_{p_0} \left[ \frac{p_1}{p_0} \right] = \frac{1 - \pi_0}{\pi_0},$$

since  $\mathbb{E}_{H_0} \left[ \frac{r(\hat{\beta})}{p_0(\hat{\beta})} \right] = \int \frac{r(\hat{\beta})}{p_0(\hat{\beta})} p_0(\hat{\beta}) d\hat{\beta} = \int r(\hat{\beta}) d\hat{\beta} = 1$  for any density  $r$ . Because  $x \mapsto \frac{1-x}{x}$  is strictly decreasing on  $(0, 1)$  and  $\tilde{\pi}_0 \geq \pi_0$ , the claim follows.  $\square$

Under the alternative, conservativeness is seen via an analogous argument applied to  $\log\text{PO}$ .

**Lemma S2:** *If  $\tilde{\pi}_0 \geq \pi_0$ , then*

$$\mathbb{E}_{H_1}[\log \widetilde{\text{PO}}] \leq \mathbb{E}_{H_1}[\log \text{PO}].$$

*Proof.* Under  $H_1$ ,

$$\begin{aligned} \mathbb{E}_{H_1}[\log \widetilde{\text{PO}}] &= \log \frac{1 - \tilde{\pi}_0}{\tilde{\pi}_0} + \mathbb{E}_{p_1} \left[ \log \frac{\tilde{p}_1}{p_0} \right] \\ &= \log \frac{1 - \tilde{\pi}_0}{\tilde{\pi}_0} + \mathbb{E}_{p_1} \left[ \log \frac{p_1}{p_0} \right] - \mathbb{E}_{p_1} \left[ \log \frac{p_1}{\tilde{p}_1} \right] \\ &= \log \frac{1 - \tilde{\pi}_0}{\tilde{\pi}_0} + D_{\text{KL}}(p_1 \| p_0) - D_{\text{KL}}(p_1 \| \tilde{p}_1) \\ &\leq \log \frac{1 - \tilde{\pi}_0}{\tilde{\pi}_0} + D_{\text{KL}}(p_1 \| p_0) \leq \log \frac{1 - \pi_0}{\pi_0} + D_{\text{KL}}(p_1 \| p_0) = \mathbb{E}_{H_1}[\log \text{PO}], \end{aligned}$$

since  $D_{\text{KL}}(\cdot \| \cdot) \geq 0$  and  $x \mapsto \log \frac{1-x}{x}$  is strictly decreasing on  $(0, 1)$  with  $\tilde{\pi}_0 \geq \pi_0$ .  $\square$

## Appendix C: Simulation Study

We conducted a simulation study to evaluate the performance of FASH with the proposed BF-based adjustment for estimating the null proportion  $\pi_0$ . The two hypothesis settings were testing whether the effect function is constant or linear, consistent with Section 4.

We generated  $J = 1000$  independent observation units, each with an effect function  $\beta_j$  drawn from one of the following three categories:

- A. *Non-dynamic*:  $\beta_j = c_j$  with  $c_j \sim N(0, 1)$ .
- B. *Linear-dynamic*:  $\beta_j = c_j + b_j t$  with  $c_j \sim N(0, 1)$  and  $b_j \sim N(0, 1/4)$ .
- C. *Nonlinear-dynamic*:  $\beta_j$  sampled from a standard  $IWP_2(\sigma)$  with  $\sigma(16) = 5$ .

Each function was observed at sixteen equally spaced time points  $t = 0, 1, \dots, 16$ . Standard errors  $s_{j,r}$  were drawn independently from  $\{0.1, 0.3, 0.5\}$  with equal probability. Examples of simulated observations are shown in Fig. S1. To vary the underlying null proportion, we introduced a parameter  $\rho \in [0.05, 0.5]$  with increment 0.01. For each  $\rho$ , we simulated  $J(1 - \rho)$  observations from category A,  $J\rho/2$  from category B, and the remainder from category C. Thus, when testing  $S_0$  as constant functions, the true null proportion is  $\pi_0 = 1 - \rho$ , and when testing  $S_0$  as linear functions, the true null proportion is  $\pi_0 = 1 - \rho/2$ .

We fit the FASH model as in Section 4, and compared the unpenalized MLE  $\hat{\pi}_0$  with its BF-adjusted counterpart. Results are summarized in Fig. S2. Panels (a-b) demonstrate that the BF-adjusted estimates consistently remain above the true  $\pi_0$  across replications, confirming the conservative property stated in Theorem 1. In contrast, the raw MLE often underestimates  $\pi_0$ , particularly when testing  $S_0$  as constant functions. Panels (c-d) further show that using a denser grid for  $\sigma$  does not affect this conclusion: the BF-adjusted estimates still maintain the desired conservativeness.

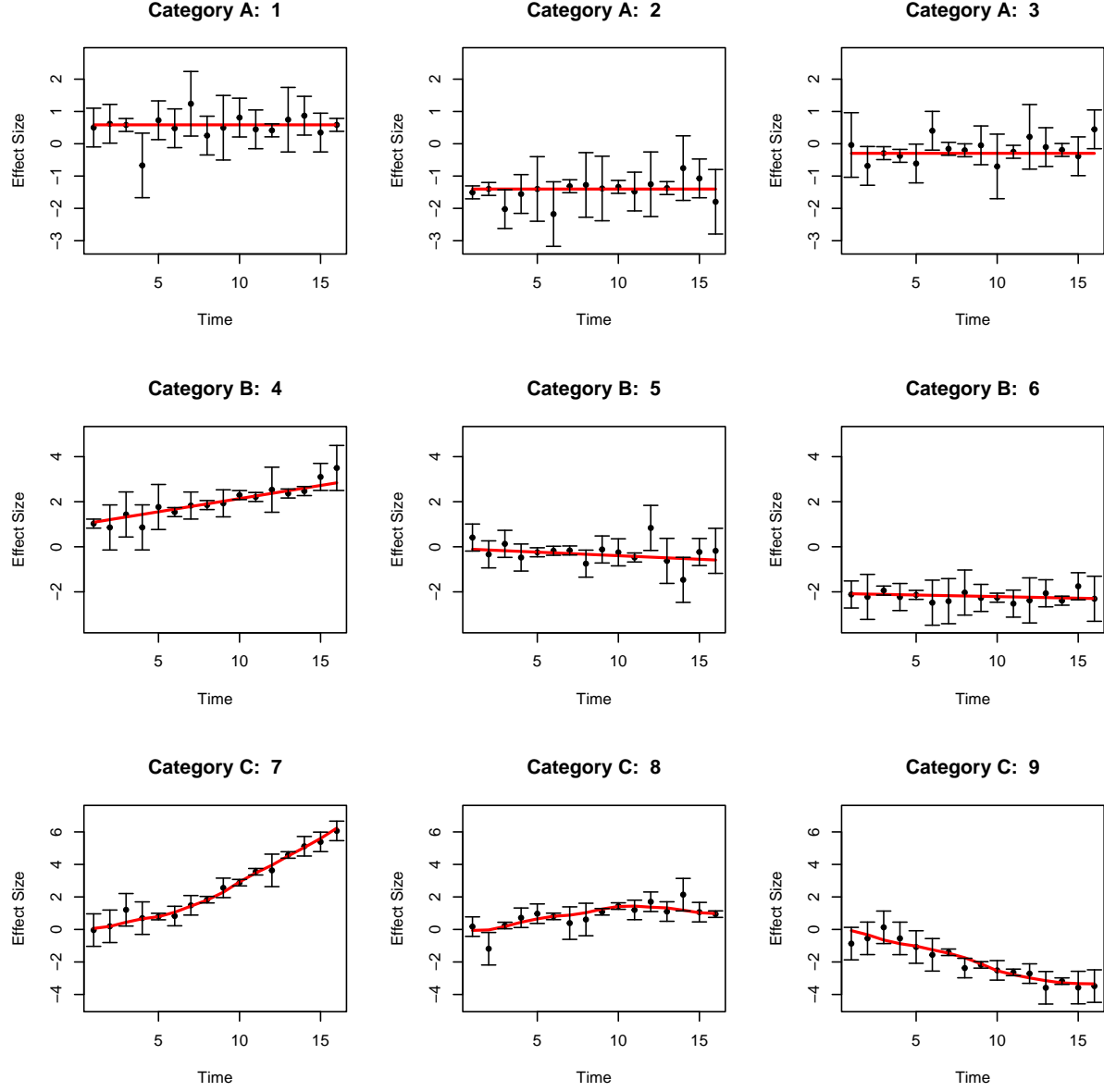


Figure S1: Examples of simulated observations: points indicate observed effect estimates; vertical bars denote  $\pm 2$  standard errors; red lines denote the true effect function  $\beta_j$ .

Next, we examine a specific setting with  $\rho = 0.2$ , which corresponds to a true null proportion of  $\pi_0 = 0.8$  when testing for dynamic eQTLs and  $\pi_0 = 0.9$  when testing for nonlinear dynamic eQTLs. We apply FASH as in Section 4 to address two inferential goals: (i) detecting dynamic eQTLs and (ii) detecting nonlinear dynamic eQTLs. For a range of nominal FDR levels  $\alpha$ , we evaluate the empirical FDR of FASH with and without BF-adjustment. As shown in Fig. S3, when  $\alpha \leq 0.05$ , the empirical FDR is already well controlled without adjustment.

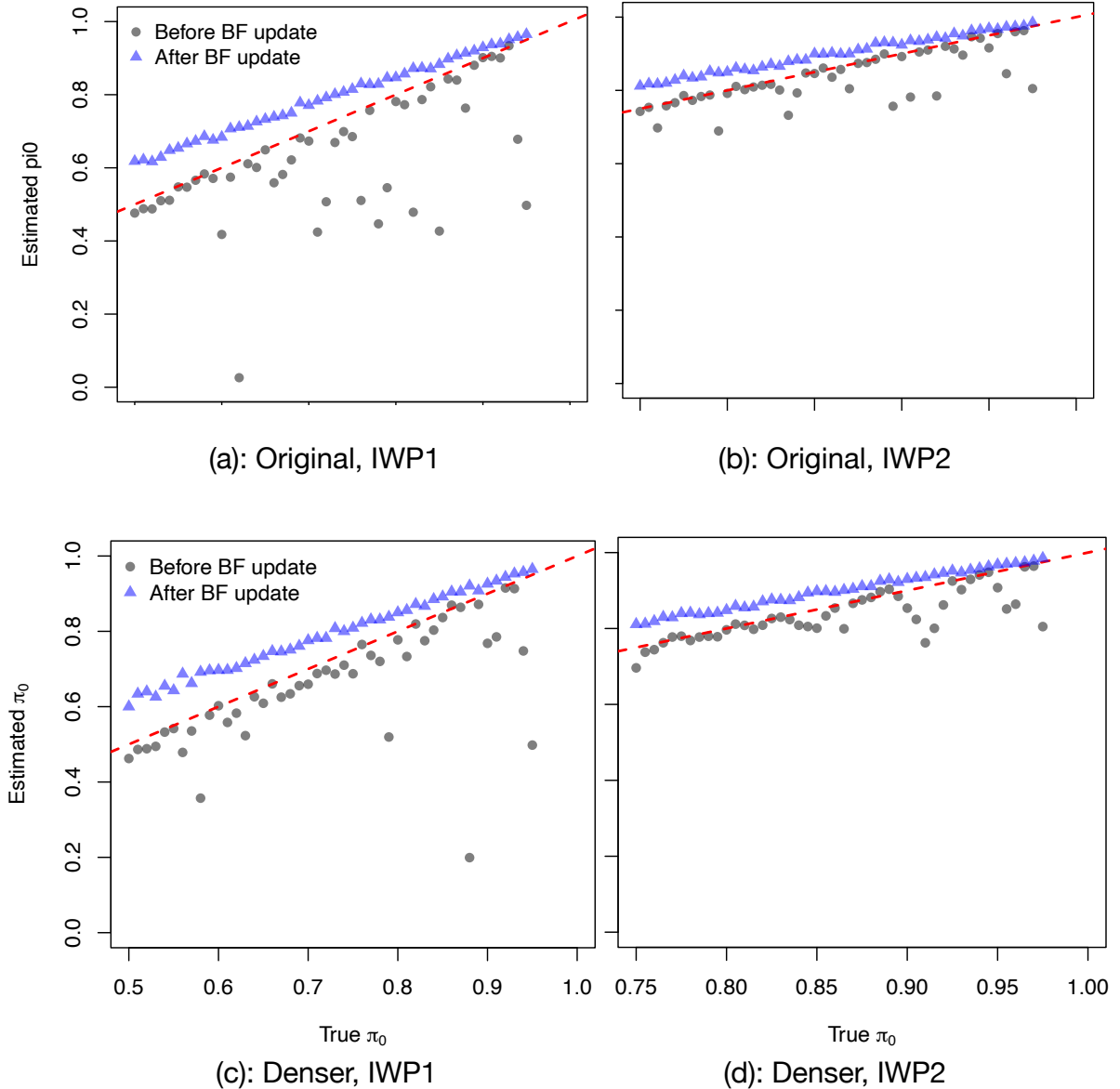


Figure S2: Estimated null proportions  $\hat{\pi}_0$  in the simulation study. The left column corresponds to testing constant functions ( $S_0 = \text{constant}$ , fitted with IWP<sub>1</sub>); the right column corresponds to testing linear functions ( $S_0 = \text{linear}$ , fitted with IWP<sub>2</sub>). Black: MLE; blue: BF-adjusted estimates; red: 45-degree line. (a-b) results using the original grid in Section 4 (spacing 0.2 on log-precision scale). (c-d) results using a denser grid (spacing 0.1).

However, as  $\alpha$  increases, the unadjusted results exhibit inflated FDR, particularly when testing for nonlinear dynamic eQTLs. In contrast, the BF-adjusted version consistently controls FDR at or below the nominal level, in agreement with the theoretical guarantee of Theorem 1.

In terms of power, the BF-adjustment yields slightly more conservative results, leading to a modest reduction in power. This loss, however, is small—capped at about 5% in the worst case—and the BF-adjusted FASH still achieves over 80% power when  $\alpha = 0.05$  for both tasks. Therefore, we view this as a reasonable trade-off to ensure FDR remains below the nominal level, and recommend applying the BF-adjustment in practice. Examples of significant discoveries at  $\alpha = 0.05$  are shown in Fig. S4, with the posterior effect functions obtained from FASH compared against the true underlying effects.

## Appendix D: Additional Details of the iPSC Cardiomyocyte Differentiation Study

For each gene-variant pair  $j \in [J]$ , we obtained eQTL effect estimates  $\hat{\beta}_j(t_r)$  at 16 time points by fitting linear regression models, separately at each time point  $r \in [16]$ . We used the same linear regression model that was used in Strober et al. (2019):

$$E_{jc}(t_r) \mid \mathbf{z}_{cr}, G_c \stackrel{\text{ind}}{\sim} N(\mathbf{z}_{cr}^T \mathbf{b}_{jr} + G_c \beta_j(t_r), \sigma_{E_{jr}}^2), \quad r \in [16], c \in [C_r], j \in [J], \quad (31)$$

in which  $E_{jc}(t_r) \in \mathbb{R}$  denotes the standardized expression of gene  $j$  in cell line  $c$  at time point  $t_r$ ,  $G_c \in \{0, 1, 2\}$  is the genotype dosage of the SNP in cell line  $c$ ,  $\mathbf{z}_{cr} \in \mathbb{R}^6$  is the vector of covariates (intercept and first 5 PCs), and  $\beta_j(t_r) \in \mathbb{R}$ ,  $\mathbf{b}_{jr} \in \mathbb{R}^6$  are the regression coefficients to be estimated. Principal components (PCs) were computed from the “cell-line-collapsed” expression matrix of dimension  $19 \times 212,147$  (Strober et al., 2019). The number of cell lines observed at time  $t_r$ , denoted by  $C_r$ , was 19 for most time points, except for day 14 (18 cell lines) and days 3 and 5 (16 cell lines). The residual variance  $\sigma_{E_{jr}}^2$  at time point  $t_r$  was assumed to be constant across cell lines at a given time point. From (31), we computed the  $t$  statistic for each gene-variant pair on each day as  $T_{jr} = \hat{\beta}_j(t_r)/s_{jr}$ , in which  $s_{jr}$  is the standard error of  $\hat{\beta}_j(t_r)$ .

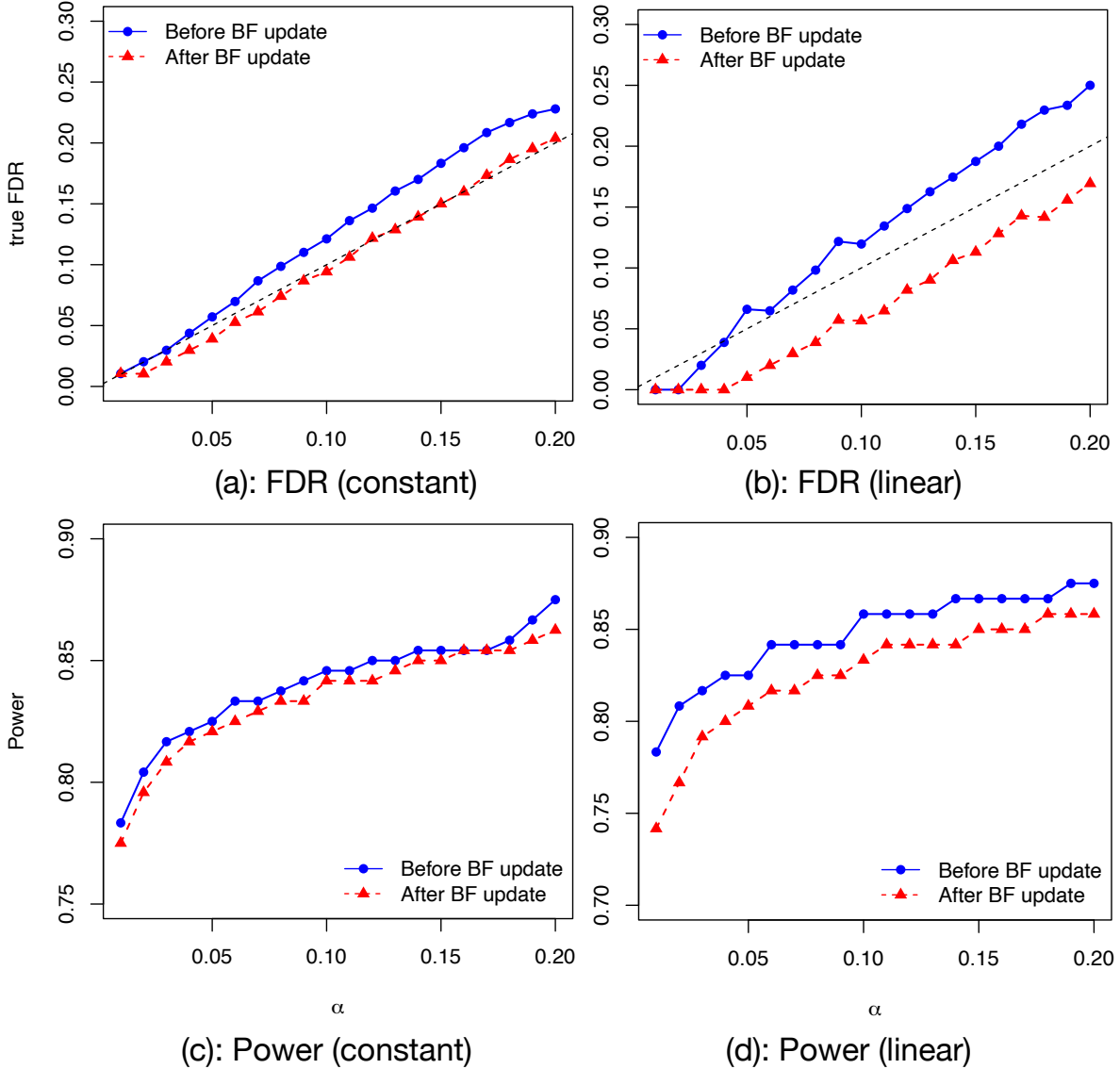


Figure S3: Empirical FDR (a-b) and power (c-d) of FASH under the two inferential goals, plotted against the nominal FDR  $\alpha$ , with (red) or without (blue) the BF-adjustment of  $\pi_0$ . The left column corresponds to testing dynamic eQTLs ( $H_0 : \beta_j$  constant), and the right column to testing nonlinear dynamics ( $H_0 : \beta_j$  linear). The black dashed line in (a-b) is the 45-degree reference line for FDR calibration.

Under the null hypothesis that  $\beta_j(t_r) = 0$ ,  $T_{jr}$  follows a  $t$  distribution with  $\nu_r = C_r - 5$  degrees of freedom. If the number of cell lines measured at each time point were large, the asymptotic normality of the maximum-likelihood estimator would imply that  $T_{jr}$  approximately follows a standard normal distribution, and hence  $\hat{\beta}_j(t_r) \sim N(\beta_j(t_r), s_{jr}^2)$ . However, since only 19 cell lines were included in this study, this approximation is not reliable. In fact, inflation of

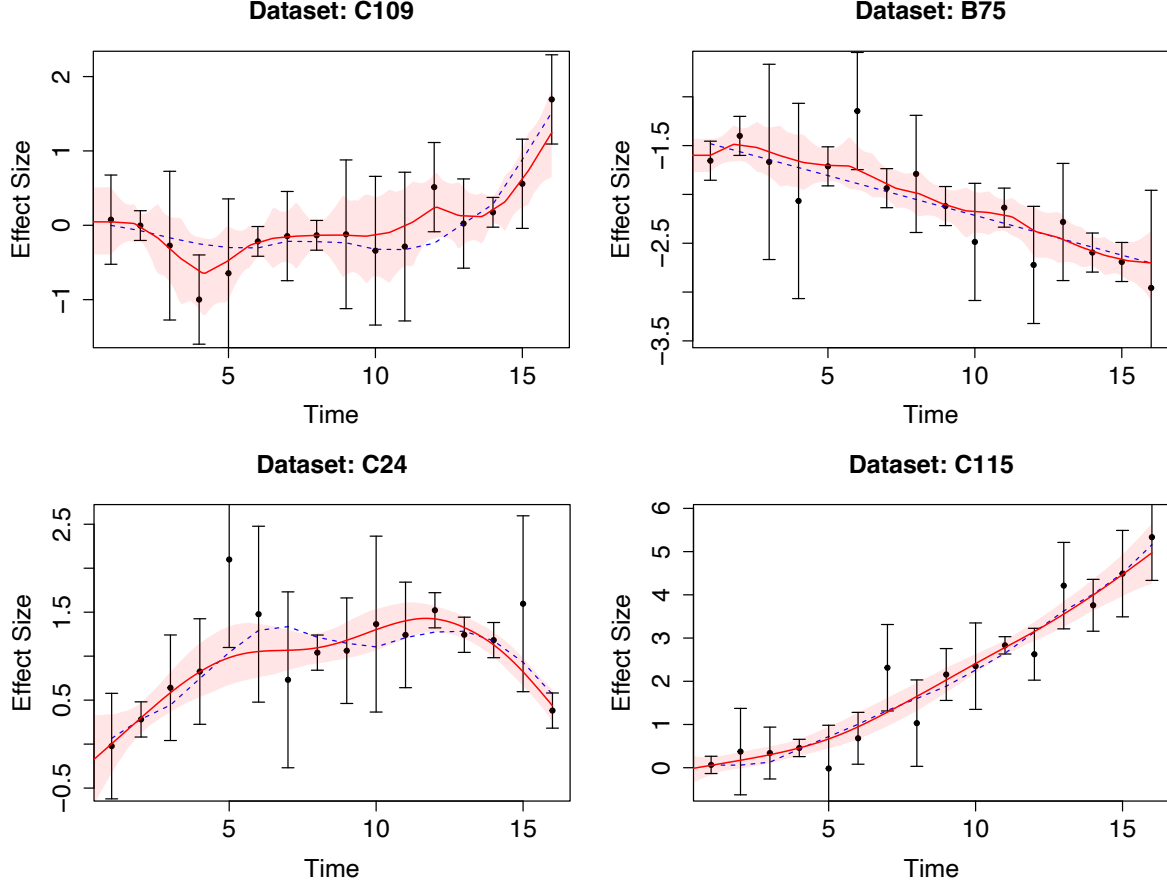


Figure S4: Examples of significant eQTLs identified by FASH in the simulation study at a nominal FDR level of  $\alpha = 0.05$  (top: dynamic eQTLs; bottom: nonlinear < dynamic eQTLs). The posterior mean of  $\beta_j$  is shown as a red solid line, with the 95% credible interval shaded in red. Observed effect size estimates  $\hat{\beta}_j$  are shown as black dots with error bars denoting  $\pm 2\tilde{s}_{jr}$ . The true underlying effect function is shown as a blue dashed line.

the type I error rate was reported under this setting (see Fig. S10 in the supplement of Strober et al. 2019). To account inflation of type I error  $\alpha$  in a scalable way, following (Lu and Stephens, 2019) we defined “ $t$ -adjusted standard errors”  $\tilde{s}_{jr}$  as satisfying

$$\Phi(\hat{\beta}_j(t_r)/\tilde{s}_{jr}) = P_{T_{\nu_r}}(\hat{\beta}_j(t_r)/s_{jr}), \quad (32)$$

where  $\Phi$  denotes the CDF of the standard normal distribution and  $P_{T_{\nu_r}}$  is the CDF of the  $t$  distribution with  $\nu_r$  degrees of freedom. The effect estimates  $\hat{\beta}_{jr}$  and the adjusted standard errors  $\tilde{s}_{jr}$  were then the inputs to FASH.

The priors (10) used in the the FASH analyses were all defined on an equally spaced grid on the log-scale, with  $\sigma_0 = 0, \sigma_1 = e^{-5} \approx 0.01, \sigma_{52} = 1$ , and  $\log \sigma_{k+1} = \log \sigma_k + 0.1$ ,  $k = 2, \dots, 51$ .

## Appendix E: Supplementary Figures & Tables

Table 3: Gene-set enrichment results for highlighted genes with dynamic eQTLs (Dynamic) and for genes with switch dynamic eQTLs (Switch). All gene sets are from the MSigDB Hallmark (HALLMARK\_\*) collection; the prefix is omitted in the table.

Category	Gene set	GeneRatio	BgRatio	p-value	q-value
Dynamic	HYPOXIA	25/1177	89/6362	0.0169	0.436
Dynamic	IL6_JAK_STAT3_SIGNALING	8/1177	21/6362	0.0280	0.436
Dynamic	ESTROGEN_RESPONSE_EARLY	22/1177	82/6362	0.0394	0.436
Dynamic	ESTROGEN_RESPONSE_LATE	21/1177	79/6362	0.0476	0.436
Dynamic	ANDROGEN_RESPONSE	16/1177	57/6362	0.0499	0.436
Dynamic	HEME_METABOLISM	22/1177	85/6362	0.0564	0.436
Dynamic	NOTCH_SIGNALING	5/1177	15/6362	0.1276	0.750
Dynamic	KRAS_SIGNALING_DN	8/1177	28/6362	0.1306	0.750
Dynamic	GLYCOLYSIS	23/1177	100/6362	0.1498	0.750
Dynamic	MYOGENESIS	16/1177	67/6362	0.1624	0.750
Dynamic	UV_RESPONSE_DN	16/1177	68/6362	0.1780	0.750
Dynamic	KRAS_SIGNALING_UP	11/1177	47/6362	0.2415	0.840
Dynamic	TNFA_SIGNALING_VIA_NFKB	13/1177	58/6362	0.2665	0.840
Dynamic	HEDGEHOG_SIGNALING	4/1177	15/6362	0.2962	0.840
Dynamic	APOPTOSIS	15/1177	70/6362	0.3072	0.840
Dynamic	INTERFERON_GAMMA_RESPONSE	12/1177	56/6362	0.3359	0.840
Dynamic	MITOTIC_SPINDLE	28/1177	139/6362	0.3399	0.840
Dynamic	WNT_BETA_CATENIN_SIGNALING	5/1177	21/6362	0.3455	0.840

Category	Gene set	GeneRatio	BgRatio	p-value	q-value
Dynamic	COAGULATION	7/1177	31/6362	0.3459	0.840
Dynamic	P53_PATHWAY	17/1177	83/6362	0.3626	0.840
Dynamic	ADIPOGENESIS	20/1177	106/6362	0.5008	0.945
Dynamic	REACTIVE_OXYGEN_SPECIES_PATHWAY	5/1177	26/6362	0.5410	0.945
Dynamic	APICAL_SURFACE	3/1177	15/6362	0.5439	0.945
Dynamic	PI3K_AKT_MTOR_SIGNALING	10/1177	55/6362	0.5794	0.945
Dynamic	COMPLEMENT	10/1177	57/6362	0.6278	0.945
Dynamic	IL2_STAT5_SIGNALING	13/1177	75/6362	0.6499	0.945
Dynamic	XENOBIOTIC_METABOLISM	12/1177	71/6362	0.6837	0.945
Dynamic	INTERFERON_ALPHA_RESPONSE	4/1177	27/6362	0.7633	0.945
Dynamic	APICAL_JUNCTION	13/1177	82/6362	0.7739	0.945
Dynamic	DNA_REPAIR	13/1177	82/6362	0.7739	0.945
Dynamic	ANGIOGENESIS	2/1177	15/6362	0.7956	0.945
Dynamic	EPITHELIAL_MESENCHYMAL_TRANSITION	13/1177	84/6362	0.8031	0.945
Dynamic	PROTEIN_SECRETION	9/1177	61/6362	0.8208	0.945
Dynamic	ALLOGRAFT_REJECTION	5/1177	36/6362	0.8225	0.945
Dynamic	TGF_BETA_SIGNALING	5/1177	36/6362	0.8225	0.945
Dynamic	UNFOLDED_PROTEIN_RESPONSE	11/1177	75/6362	0.8442	0.945
Dynamic	FATTY_ACID_METABOLISM	10/1177	72/6362	0.8812	0.945
Dynamic	MYC_TARGETS_V2	5/1177	41/6362	0.8992	0.945
Dynamic	BILE_ACID_METABOLISM	3/1177	28/6362	0.9132	0.945
Dynamic	SPERMATOGENESIS	3/1177	28/6362	0.9132	0.945
Dynamic	UV_RESPONSE_UP	10/1177	76/6362	0.9174	0.945
Dynamic	INFLAMMATORY_RESPONSE	5/1177	43/6362	0.9206	0.945
Dynamic	OXIDATIVE_PHOSPHORYLATION	16/1177	119/6362	0.9445	0.945
Dynamic	PEROXISOME	4/1177	44/6362	0.9739	0.945

Category	Gene set	GeneRatio	BgRatio	p-value	q-value
Dynamic	G2M_CHECKPOINT	16/1177	136/6362	0.9881	0.945
Dynamic	MTORC1_SIGNALING	13/1177	129/6362	0.9973	0.945
Dynamic	CHOLESTEROL_HOMEOSTASIS	2/1177	42/6362	0.9981	0.945
Dynamic	E2F_TARGETS	10/1177	127/6362	0.9998	0.945
Dynamic	MYC_TARGETS_V1	6/1177	124/6362	1.0000	0.945
Switch	HYPOXIA	11/250	89/6362	0.000668	0.0246
Switch	KRAS_SIGNALING_UP	7/250	47/6362	0.00218	0.0348
Switch	MYOGENESIS	8/250	67/6362	0.00445	0.0348
Switch	P53_PATHWAY	9/250	83/6362	0.00501	0.0348
Switch	GLYCOLYSIS	10/250	100/6362	0.00565	0.0348
Switch	ANDROGEN_RESPONSE	7/250	57/6362	0.00656	0.0348
Switch	COAGULATION	5/250	31/6362	0.00662	0.0348
Switch	IL6_JAK_STAT3_SIGNALING	4/250	21/6362	0.00822	0.0378
Switch	NOTCH_SIGNALING	3/250	15/6362	0.0192	0.0787
Switch	APICAL_JUNCTION	7/250	82/6362	0.0415	0.153
Switch	INTERFERON_GAMMA_RESPONSE	5/250	56/6362	0.0678	0.227
Switch	REACTIVE_OXYGEN_SPECIES_PATHWAY	3/250	26/6362	0.0802	0.246
Switch	ESTROGEN_RESPONSE_LATE	6/250	79/6362	0.0894	0.253
Switch	ESTROGEN_RESPONSE_EARLY	6/250	82/6362	0.1025	0.268
Switch	EPITHELIAL_MESENCHYMAL_TRANSITION	6/250	84/6362	0.1117	0.268
Switch	HEME_METABOLISM	6/250	85/6362	0.1165	0.268
Switch	APOPTOSIS	5/250	70/6362	0.1398	0.299
Switch	XENOBIOTIC_METABOLISM	5/250	71/6362	0.1459	0.299
Switch	PI3K_AKT_MTOR_SIGNALING	4/250	55/6362	0.1690	0.328
Switch	TNFA_SIGNALING_VIA_NFKB	4/250	58/6362	0.1927	0.355
Switch	MYC_TARGETS_V2	3/250	41/6362	0.2171	0.381

Category	Gene set	GeneRatio	BgRatio	p-value	q-value
Switch	INFLAMMATORY_RESPONSE	3/250	43/6362	0.2380	0.399
Switch	UV_RESPONSE_DN	4/250	68/6362	0.2778	0.445
Switch	KRAS_SIGNALING_DN	2/250	28/6362	0.3018	0.463
Switch	UNFOLDED_PROTEIN_RESPONSE	4/250	75/6362	0.3405	0.502
Switch	COMPLEMENT	3/250	57/6362	0.3895	0.529
Switch	MTORC1_SIGNALING	6/250	129/6362	0.3964	0.529
Switch	ALLOGRAFT_REJECTION	2/250	36/6362	0.4164	0.529
Switch	TGF_BETA_SIGNALING	2/250	36/6362	0.4164	0.529
Switch	HEDGEHOG_SIGNALING	1/250	15/6362	0.4523	0.555
Switch	MITOTIC_SPINDLE	6/250	139/6362	0.4670	0.555
Switch	OXIDATIVE_PHOSPHORYLATION	5/250	119/6362	0.5046	0.581
Switch	MYC_TARGETS_V1	5/250	124/6362	0.5415	0.600
Switch	WNT_BETA_CATENIN_SIGNALING	1/250	21/6362	0.5697	0.600
Switch	IL2_STAT5_SIGNALING	3/250	75/6362	0.5705	0.600
Switch	ADIPOGENESIS	4/250	106/6362	0.6043	0.618
Switch	G2M_CHECKPOINT	5/250	136/6362	0.6244	0.622
Switch	INTERFERON_ALPHA_RESPONSE	1/250	27/6362	0.6620	0.642
Switch	FATTY_ACID_METABOLISM	2/250	72/6362	0.7817	0.736
Switch	CHOLESTEROL_HOMEOSTASIS	1/250	42/6362	0.8153	0.736
Switch	PEROXISOME	1/250	44/6362	0.8297	0.736
Switch	DNA_REPAIR	2/250	82/6362	0.8392	0.736
Switch	PROTEIN_SECRETION	1/250	61/6362	0.9143	0.783
Switch	UV_RESPONSE_UP	1/250	76/6362	0.9534	0.798
Switch	E2F_TARGETS	1/250	127/6362	0.9942	0.814

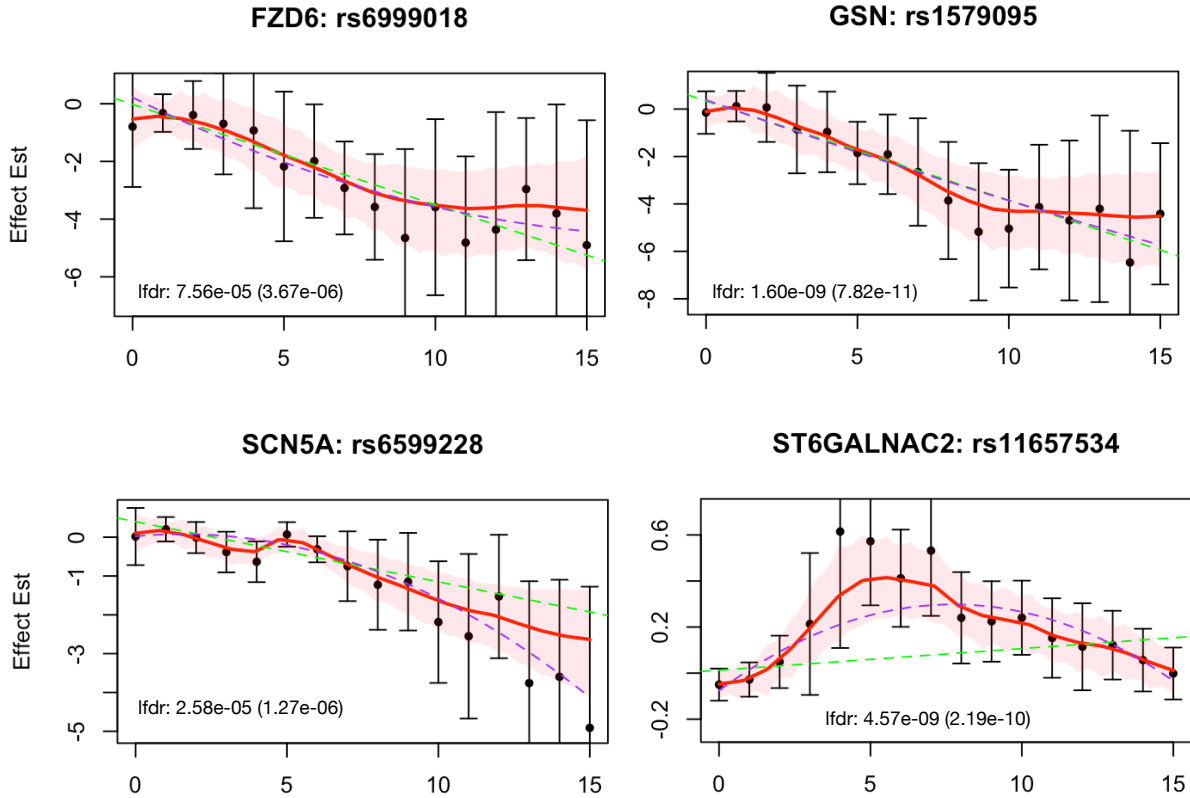


Figure S5: Selected gene-variant pairs with significant dynamic eQTL effects based on a 5% FDR threshold. In each plot, the posterior mean of  $\beta_j$  is shown as a red solid line and the 95% credible interval is shown by the red shaded region. Observed effect size estimates  $\hat{\beta}_j$  are shown as black dots and vertical bars represent  $\pm 2$  the (adjusted) standard errors  $\tilde{s}_{jr}$ . In “lfd: x (y)”, x is the lfd after the BF adjustment, and y is the lfd before the BF adjustment. For comparison, the inverse-variance weighted least squares estimates of  $\hat{\beta}_j$  are shown as green (linear) and purple (quadratic) dashed lines. Variants rs6999018 and rs1579095 appear to have minimal impact on the expression of their respective genes, *FZD6* and *GSN*, during the first three days of differentiation, but begin to significantly downregulate expression at later stages. These genes have been previously implicated in cardiomyocyte development and function. For example, Mazzotta et al. (2016) reported that *FZD6* plays an important regulatory role in cardiomyocyte differentiation through non-canonical Wnt signaling, while Li et al. (2009) showed that *GSN* contributes to cardiac remodeling via DNase I-mediated apoptosis.

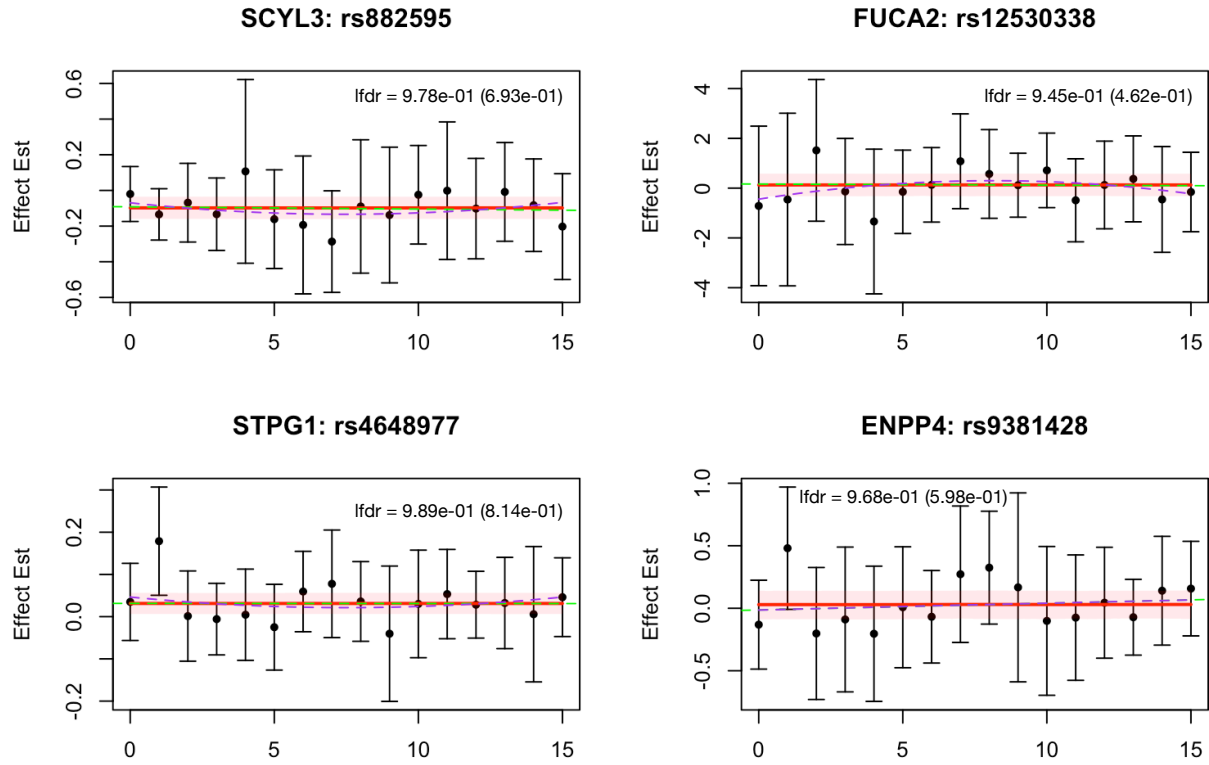


Figure S6: Selected variant-gene pairs showing no significant dynamic eQTL effects based on the 5% false discovery rate threshold. The posterior mean of  $\beta_j$  is shown as a red solid line, with the 95% credible interval indicated by the red shaded region. Observed effect size estimates  $\hat{\beta}_j$  are shown as black dots, with vertical bars representing  $\pm 2\tilde{s}_{j,r}$ . The lFdr for each pair is shown, with the value before BF adjustment given in parentheses. For comparison, inverse-variance weighted least squares estimates of  $\hat{\beta}_j$  are shown as a green dashed line (linear) and a purple dashed line (quadratic).

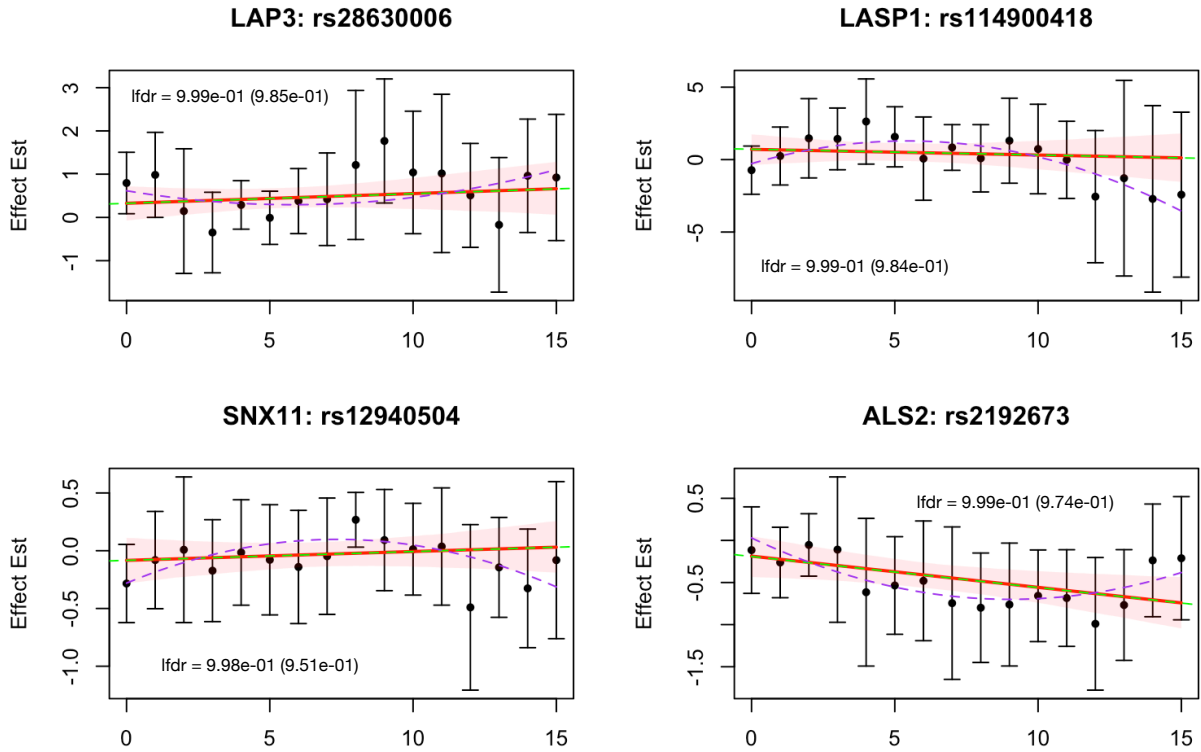


Figure S7: Selected variant-gene pairs showing no significant nonlinear dynamic eQTL effects based on the 5% false discovery rate threshold. The posterior mean of  $\beta_j$  is shown as a red solid line, with the 95% credible interval indicated by the red shaded region. Observed effect size estimates  $\hat{\beta}_j$  are shown as black dots, with vertical bars representing  $\pm 2\tilde{s}_{j,r}$ . The lfdr for each pair is shown, with the value before BF adjustment given in parentheses. For comparison, inverse-variance weighted least squares estimates of  $\hat{\beta}_j$  are shown as a green dashed line (linear) and a purple dashed line (quadratic).

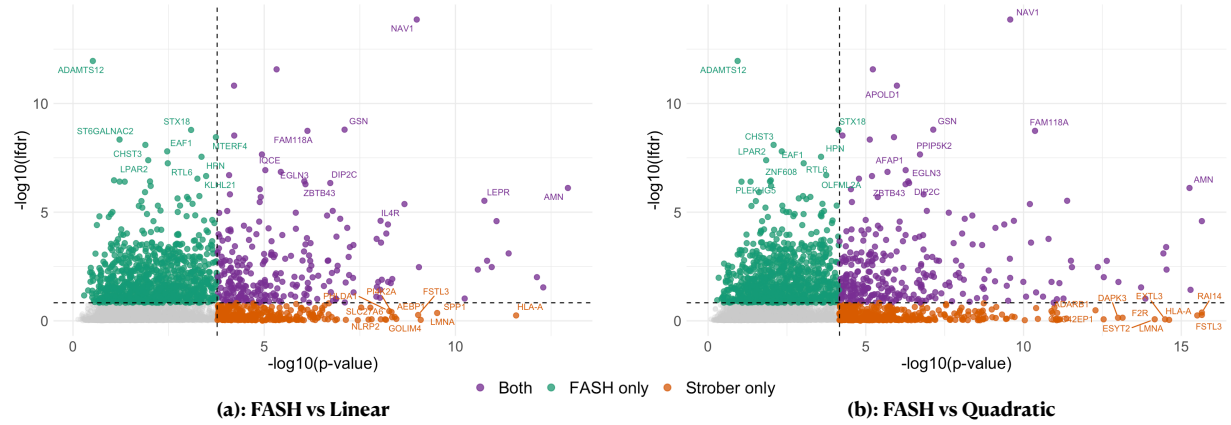


Figure S8: Scatterplot of  $(-\log_{10})$  lfdr from FASH-IWP<sub>1</sub> versus  $(-\log_{10})$  p-values from Strober et al. (2019), based on the linear (a) or quadratic interaction (b) test. Each point represents a unique gene; for each gene, the lfdr and p-value are taken from the variant-gene pair with the smallest lfdr and the smallest p-value, respectively. The horizontal dashed line indicates the lfdr cutoff corresponding to FDR = 0.05. The colors indicate significance relative to the FDR threshold (grey: significant in neither; green: significant only by lfdr; orange: significant only by p-value; purple: significant in both).

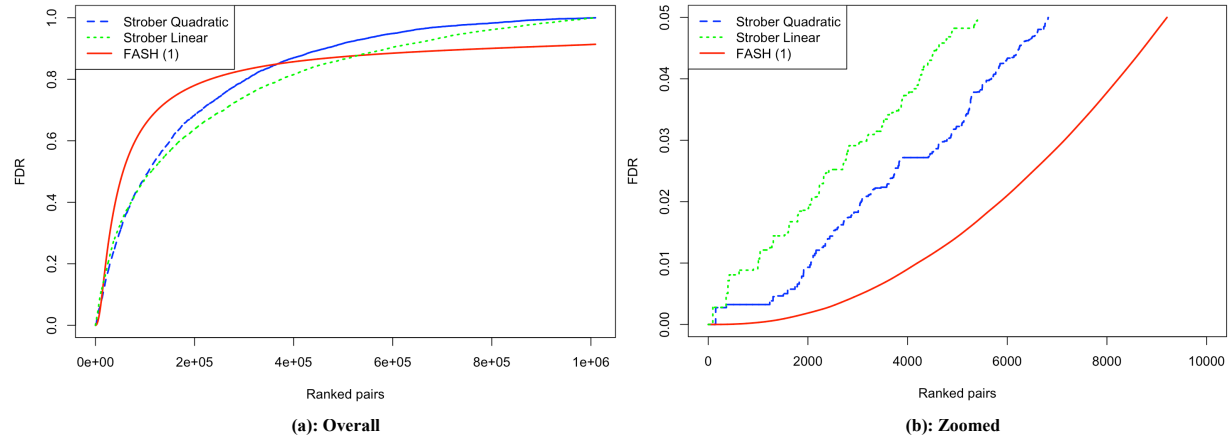


Figure S9: False discovery rate (FDR) along the ranked list of variant-gene pairs (from most to least significant), computed from the local false discovery rates (lfdrs) produced by FASH-IWP<sub>1</sub> (solid red) and by applying the eFDR procedure of Gamazon et al. (2013) to the p-values reported in Strober et al. (2019) (linear test: dotted green; quadratic test: dashed blue).

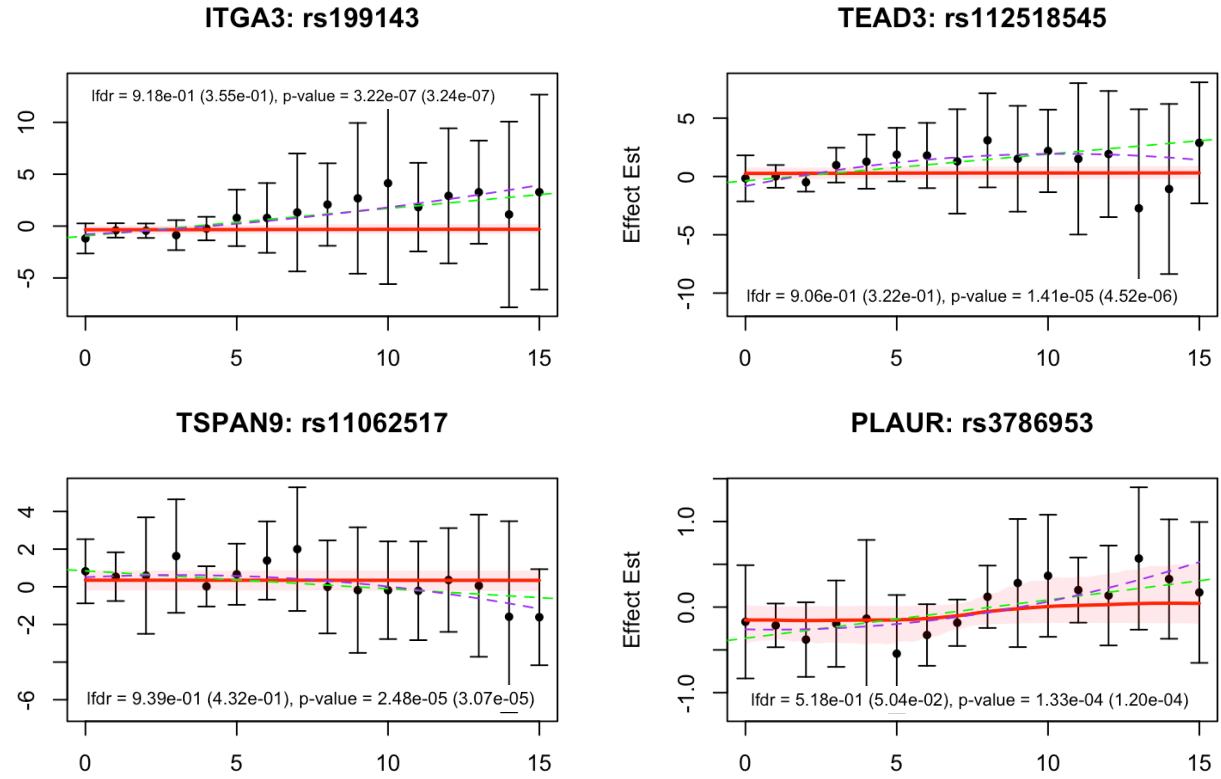


Figure S10: Examples of genes identified in Strober et al. (2019) but not detected by FASH-IWP<sub>1</sub>. For each variant-gene pair, the posterior mean of  $\beta_j$  is shown as a solid red line, with the 95% credible interval indicated by the red shaded band. Observed effect size estimates  $\hat{\beta}_j$  are shown as black dots, with vertical bars representing  $\pm 2\tilde{s}_{j,r}$ . The Ifdr for each pair is reported, with the pre-BF-adjustment value shown in parentheses. The (linear/quadratic) p-values from Strober et al. (2019) are also reported, with the quadratic p-value shown in parentheses.